NAVAL POSTGRADUATE SCHOOL

MONTEREY, CALIFORNIA

THESIS

CHARACTERIZATION OF EHTYLENE/JP-10 FUEL INJECTION PROFILES FOR A VALVELESS PULSE DETONATION ENGINE

by

Thomas J. Danaher

December 2007

Thesis Advisor:	Christopher Brophy
Second Reader:	Jose O. Sinibaldi

Approved for public release; distribution is unlimited

THIS PAGE INTENTIONALLY LEFT BLANK

REPORT DOCUMENTATION PAGE			Form Approved OMB No. 0704-0188
Public reporting burden for this collection of information is estimated to average 1 hour per response, including the time for reviewing instruction, searching existing data sources, gathering and maintaining the data needed, and completing and reviewing the collection of information. Send comments regarding this burden estimate or any other aspect of this collection of information, including suggestions for reducing this burden, to Washington headquarters Services, Directorate for Information Operations and Reports, 1215 Jefferson Davis Highway, Suite 1204, Arlington, VA 22202-4302, and to the Office of Management and Budget, Paperwork Reduction Project (0704-0188) Washington DC 20503.			
1. AGENCY USE ONLY ***(Leave blank)***	**2. REPORT DATE** December 2007	**3. REPORT TYPE AND DATES COVERED** Master's Thesis	
4. TITLE AND SUBTITLE Characterization of Ethylene/JP-10 Fuel Injection Profiles for a Valveless Pulse Detonation Engine.		**5. FUNDING NUMBERS**	
6. AUTHOR(S) Thomas Danaher			
7. PERFORMING ORGANIZATION NAME(S) AND ADDRESS(ES) Naval Postgraduate School Monterey, CA 93943-5000		**8. PERFORMING ORGANIZATION REPORT NUMBER**	
9. SPONSORING /MONITORING AGENCY NAME(S) AND ADDRESS(ES) N/A		**10. SPONSORING/MONITORING AGENCY REPORT NUMBER**	
11. SUPPLEMENTARY NOTES The views expressed in this thesis are those of the author and do not reflect the official policy or position of the Department of Defense or the U.S. Government.			
12a. DISTRIBUTION / AVAILABILITY STATEMENT Approved for public release; distribution is unlimited		**12b. DISTRIBUTION CODE**	

13. ABSTRACT (maximum 200 words)

Practical use of the pulse detonation engine as a form of propulsion for future aircraft and missile platforms depends upon the ability to reliably detonate a fuel air mixture at high frequencies in order to produce an acceptable level of thrust, and to take advantage of the higher thermodynamic efficiency available from the pulse detonation engine combustion cycle.

This research thesis focused on improving and mapping fuel fraction delivery profiles for a valveless pulse detonation engine. The gas dynamic conditions downstream of inlet manifold isolation chokes were evaluated for a number of geometries with Computational Fluid Dynamics software in an effort to reduce areas of recirculation in the inlet manifold of the engine and improve fuel delivery profiles. Based on the results from this modeling a new inlet manifold configuration was designed, installed and evaluated in laboratory experimentation.

Laboratory testing was performed at multiple air and fuel mass flow rates using ethylene as the fuel. Absorption spectroscopy, using a He-Ne laser tuned at the 3.39μm wavelength and known spectroscopic fuel absorption cross sections, was used to measure fuel mass fraction profiles for each engine inlet geometry at various flow rates. Additionally, JP10 fuel concentration profiles were determined for several fuel injector actuation pressures and at various alignments using the same diagnostic approach.

14. SUBJECT TERMS Pulse Detonation Engine, PDE, PDE fuel profile.			**15. NUMBER OF PAGES** 81
			16. PRICE CODE
17. SECURITY CLASSIFICATION OF REPORT Unclassified	**18. SECURITY CLASSIFICATION OF THIS PAGE** Unclassified	**19. SECURITY CLASSIFICATION OF ABSTRACT** Unclassified	**20. LIMITATION OF ABSTRACT** UU

NSN 7540-01-280-5500 Standard Form 298 (Rev. 2-89)
Prescribed by ANSI Std. 239-18

THIS PAGE INTENTIONALLY LEFT BLANK

Approved for public release; distribution is unlimited

CHARACTERIZATION OF ETHYLENE/JP-10 FUEL INJECTION PROFILES FOR A VALVELESS PULSE DETONATION ENGINE

Thomas J. Danaher
Lieutenant, United States Navy
B. Nuclear Eng. Tech., Thomas Edison State College, 2000

Submitted in partial fulfillment of the
requirements for the degree of

MASTER OF SCIENCE IN MECHANICAL ENGINEERING

from the

NAVAL POSTGRADUATE SCHOOL
December 2007

Author: Thomas J. Danaher

Approved by: Christopher M. Brophy
Thesis Advisor

Jose O. Sinibaldi
Second Reader

Anthony J. Healey
Chairman, Department of Mechanical and Astronautical Engineering

THIS PAGE INTENTIONALLY LEFT BLANK

ABSTRACT

Practical use of the pulse detonation engine as a form of propulsion for future aircraft and missile platforms depends upon the ability to reliably detonate a fuel air mixture at high frequencies in order to produce an acceptable level of thrust, and to take advantage of the higher thermodynamic efficiency available from the pulse detonation engine combustion cycle.

This research thesis focused on improving and mapping fuel fraction delivery profiles for a valveless pulse detonation engine. The gas dynamic conditions downstream of inlet manifold isolation chokes were evaluated for a number of geometries with Computational Fluid Dynamics software in an effort to reduce areas of recirculation in the inlet manifold of the engine and improve fuel delivery profiles. Based on the results from this modeling a new inlet manifold configuration was designed, installed and evaluated in laboratory experimentation.

Laboratory testing was performed at multiple air and fuel mass flow rates using ethylene as the fuel. Absorption spectroscopy, using a He-Ne laser tuned to the 3.39μm wavelength with known spectroscopic fuel absorption cross sections, was used to measure fuel mass fraction profiles for each engine inlet geometry at various flow rates. Additionally, JP10 fuel concentration profiles were determined for several fuel injector actuation pressures and at various alignments using the same diagnostic approach.

THIS PAGE INTENTIONALLY LEFT BLANK

TABLE OF CONTENTS

THIS PAGE INTENTIONALLY LEFT BLANK

LIST OF FIGURES

LIST OF TABLES

THIS PAGE INTENTIONALLY LEFT BLANK

ACKNOWLEDGMENTS

The author would like to thank Professor Chris Brophy for his invaluable assistance and education provided throughout the development of this thesis; and Professor Jose Sinibaldi for his constructive revisions of this thesis. In addition the author would like to thank Mr. George Hageman, who generously contributed many hours of his time providing assistance in the lab. The efforts and support of our colleagues at the University of Southern California (USC) and Stanford University as well as our research sponsors at the Office of Naval Research (ONR) are acknowledged and truly appreciated.

THIS PAGE INTENTIONALLY LEFT BLANK

I. INTRODUCTION

Interest in the use of detonation as a form of propulsion originated during the mid-twentieth century due to the potential for greater engine efficiency associated with the increased thermodynamic efficiency of the detonation combustion cycle. When compared to other propulsion engines, which utilize a constant pressure, or deflagration, combustion process, a detonation engine releases energy rapidly, with a lower net entropy rise for a given amount of energy released. Due to the abrupt nature of detonation events, they must occur in a repetitive manner in order to produce a quasi steady thrust. Repetitive detonations for the purpose of propulsion were first achieved at the Naval Post-graduate School in Monterey, California, in 1985 [1].

Through the use of a simple thrust tube, with a closed head end and an open downstream end, with or without a nozzle, repetitive detonations can be implemented to produce a form of propulsion. Fuel and air are injected at the beginning of each cycle and are detonated. The detonation wave produces significant head end pressure, and ultimately thrust, through momentum transfer as the detonation wave exits the thrust tube at supersonic speeds. After the detonation wave exits the tube an expansion or rarefaction wave travels from the outlet to the head end reducing pressure, venting hot combustion products and allowing a fresh charge of air to enter for the next cycle.

The thrust levels produced by the pulse detonation engine are a product of the discrete impulses provided by each detonation event, and therefore are directly dependant upon how quickly the detonation process can be repeated. The total time taken to complete a cycle determines the maximum frequency at which the engine can operate; so it is vital to characterize exactly how long each step in the PDE cycle takes in order to maximize operating frequency and thrust produced by the engine.

The operational cycle of a valve-less PDE is shown below. It begins with air flowing through the engine, removing combustion products from the previous cycle and providing a sufficient amount of purge air for the current cycle (A). Fuel is then injected into the air stream and is carried into the combustor and initiator portions of the PDE (B). Following a brief ignition delay to allow the fuel air mixture to fill the combustion

chamber and initiator, the ignition device ignites the fuel air mixture creating a deflagration in the combustion chamber (C). As the deflagration travels down the initiator tube a process called Deflagration-to-Detonation Transition (DDT) occurs and a detonation wave is formed (D). The detonation wave then progresses through the remainder of the fuel air mixture and exits the initiator tube (E). After the detonation wave exits a low pressure area is created inside the initiator and combustor leading to a rarefaction wave which rapidly travels back into the PDE venting hot combustion gasses and restoring the PDE to the condition shown in step A (F).

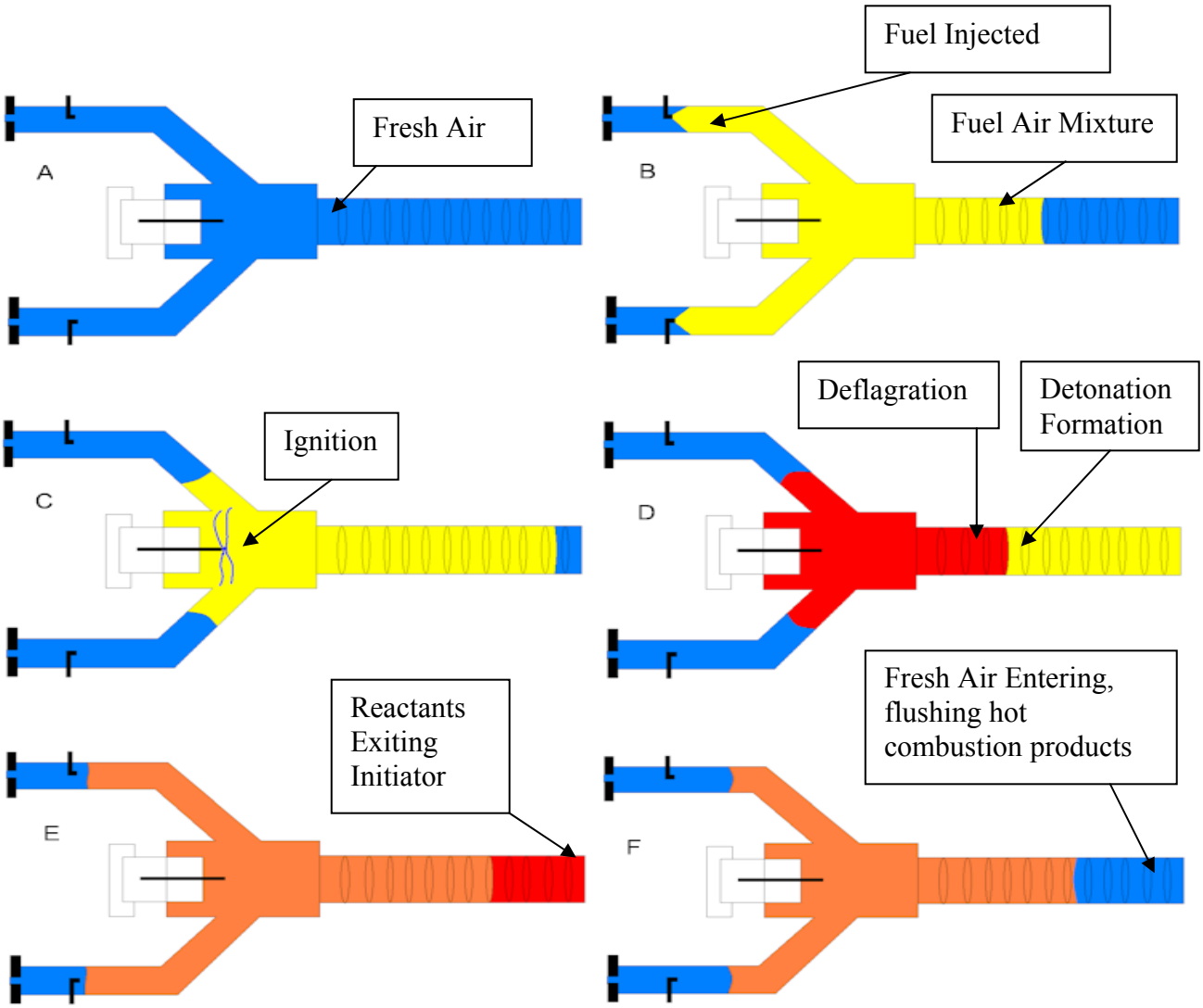

Figure 1. Pulse Detonation Engine Cycle

Each of the cycle steps described above require a period of time, dependant upon the mass flow rates through the engine, the fuel injection timing and duration, time for ignition to occur, time for DDT to occur and exit the tube and finally the time for the rarefaction wave to reduce the pressure within the chamber, expel the combustion products and purge the engine with sufficient air. The time required to purge hot combustion products from the engine is highly dependant upon engine geometry, and can be limited by recirculation zones in the engine. Failure to separate incoming reactants from residual hot combustion products can cause pre-ignition of the fuel air mixture resulting in a continuous deflagration rather than the high frequency detonations desired.

During early operational testing of the PDE, while increasing operational frequency, transition from detonations to continuous deflagration was observed. This transition was believed to be caused by insufficient purging and the recirculation of hot combustion products downstream of the inlet orifice which, due to the proximity of the fuel injectors, resulted in continuous pre-ignition of the ethylene air mixture.

The goals of this study were twofold. First flow field analysis was performed using Computational Fluid Dynamics (CFD) software to evaluate the flow field downstream of the PDE inlet orifice plates located in the inlet manifold. The results of this analysis were used in an effort to reduce recirculation downstream of the orifice while improving fuel delivery. A new inlet orifice plate was then designed, installed and evaluated. Second, spectroscopic analysis of the fuel distribution along the initiator axis was performed to evaluate fuel profiles, measure fuel mass fraction and to determine equivalence ratios for ethylene-air and JP10-air mixtures at various flow rates of both air and fuel. Fuel profiles were created and evaluated for various engine inlet geometries, and fuel mass fractions were determined for use in future performance measurement studies.

The promise of increased thermodynamic efficiency of the PDE cycle when compared to other current modes of propulsion supports further research into this technology. As shown in Figure 2, the PDE is capable of producing thrust with a specific impulse in excess of that seen in both gas turbine engines and ramjet engines when operating in a particular range of Mach numbers [2]. Turbojets demonstrate superior

performance at subsonic and low supersonic Mach numbers but their performance decreases rapidly with increasing Mach numbers. Ramjet and Scramjet Engines are capable of producing thrust with a comparable Specific Impulse at higher Mach Numbers but cannot operate at lower Mach numbers as they rely on flight speed for air compression in their inlet diffusers. The PDE combines high specific impulse with the capability to operate at both subsonic and supersonic Mach numbers therefore offering the potential to propel both missiles and aircraft.

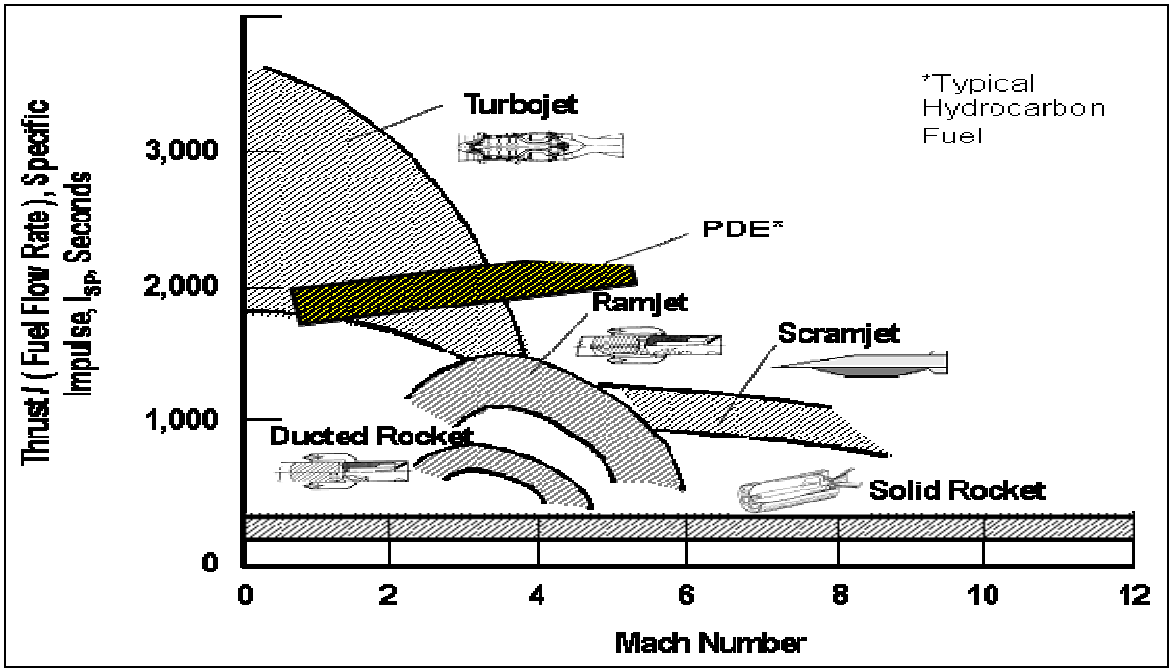

Figure 2. Comparison of High-Speed Propulsion Technologies (from [2])

These benefits, in addition to the engines relatively simple design and near absence of moving parts, provide a compelling reason for further research into Pulse Detonation as a form of propulsion.

II. BACKGROUND

A. COMBUSTION THERMODYNAMICS

Combustion is defined as an exothermic chemical reaction between a fuel and an oxidizer that once initiated can sustain itself as long as fuel and oxidizer remain in the proper proportions. An example of a complete oxygen-ethylene combustion event can be represented by:

$$C_2H_4 + 3O_2 \Leftrightarrow 2H_2O + 2CO_2 \qquad (1)$$

Assuming combustion occurs at nearly constant pressure, through a deflagration wave, the heat released during the ideal combustion event can be determined using the enthalpies of formation for reactants and products in the following manner. In this example we also assume that the reactants enter the deflagration wave at 298K and that the products are allowed to cool back to 298K.

$$H_r = H_p + Q \qquad (2)$$

$$H_r = 1kmol * (52,283kJ / kmol) + 3kmol * (0kJ / kmol)$$

$$H_p = 2kmol * (-241,827kJ / kmol) + 2kmol * (-393,522kJ / kmol)$$

$$Q_{Ideal} = 1.32kmol * 10^6 kJ / kmol$$

In reality this reaction will end in an equilibrium combustion condition in which combustion radicals and intermediates (such as OH, NO, CO etc.) will be present on the right side of equation 1. The event can be fully analyzed under the steady-state assumption using CEQUEL. CEQUEL stands for "Chemical EQUilibrium in excEL", and is based on SEA's CCET™ (Compressible Chemical Equilibrium and Transport properties) code. CCET was derived from NASA Lewis' Gordon-McBride CEA (Chemical Equilibrium with Applications) code. CEQUEL provides access to most of the capabilities available in CCET, but as an application within Microsoft Excel [8].

Entering the same ethylene-oxygen combustion event above into CEQUEL yields the following data for a stoichiometric mixture.

Table 1. CEQUEL Oxygen-Ethylene combustion data

Variable	***Units***	***Value***
Oxidizer to Fuel ratio		3.42
Fuel (percent)		22.6
Equivalence Ratio		1
Pressure	BAR	1.01
Temperature final	Degrees Kelvin	3163.7
Temperature Initial	Degrees Kelvin	273.2
Cp Products	KJ/(KG K)	1.604
Cp Reactants	KJ/(KG K)	13.3

CEQUEL assumes an adiabatic process; however, in the simplified example shown in equations 1 and 2, the products were let to cool back to 298K. Therefore to compare these results one must compute the heat release during combustion. Assuming that the specific heat at constant pressure, Cp, is constant, the heat released from the combustion event can be calculated as follows:

$$Q = Cp_{ave}(T_{final} - T_{init})kJ / kg \qquad (3)$$

$$Q = \frac{13.302 + 1.604}{2}\frac{kJ}{kg - k}(3163.7 - 273.15)K * 31.1\frac{kg}{kmol}$$

$$Q_{Real} = 6.69 * 10^5 \frac{kJ}{kmol}$$

The heat released from the equilibrium event in equation 3 is less than that released from the complete combustion in equation 2 due to the formation of free radicals. This heat release represents the net energy available from the fuel to be utilized in a propulsion device under constant pressure. While the total energy available from the fuel is constant, the manner by which it is released can be in the form of either a deflagration or a detonation.

B. COMBUSTION PROCESSES

The differences between detonations and deflagrations require clarification to fully understand the pulse detonation engine cycle. A deflagration is a combustion wave that propagates subsonically into unburned reactants. A deflagration wave occurs at near constant pressure and results in a much larger entropy rise, when compared to a detonation wave which occurs at near constant volume.

While a detonation releases about the same amount of energy as a deflagration, it does so much faster and with a lower increase in entropy, therefore providing more work potential. Combustion wave velocities for a detonation can exceed 2000m/s, several orders of magnitude larger than the typical deflagration wave which travels at 0.1 to 10 m/s.

Both the deflagration and detonation waves can be modeled as a one dimensional stationary planar wave, as shown in Figure 3 below [4]. By determining the ratio of the product properties (2) to the reactant properties (1) one can determine whether the planar wave is a detonation or a deflagration event. Typical values of these thermodynamic ratios for each event are shown below in Table 2 [5].

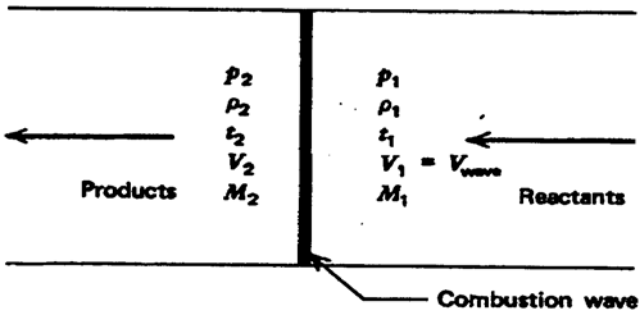

Figure 3. Stationary 1-D combustion wave (from [2])

Table 2. Qualitative Differences between Detonation and Deflagration (from [2])

	Detonation	**Deflagration**
u_1/c_1	5-10	0.0001-0.03
u_2/u_1	0.4-0.7 (deceleration)	4-16
p_2/p_1	13-55 (compression)	0.98-0.976 (slight expansion)
T_2/T_1	8-21 (heat addition)	4-16 (heat addition)
ρ_2/ρ_1	1.4-2.6	0.06-0.25

Post combustion thermodynamic properties can be determined using five primary equations.

Continuity: $(\rho av)_1 = (\rho av)_2$ (4)

Momentum: $P_1 + \rho_1 v_1^2 = P_2 + \rho_2 v_2^2$ (5)

Energy: $CpT_1 + \frac{1}{2}v_1^2 + q = CpT_2 + \frac{1}{2}v_2^2$ (6)

Ideal Gas law: $PV = nRT$ (7)

Gas Constant: $R = C_p - C_v \Rightarrow C_p = \frac{\gamma}{\gamma - 1}R$ (8)

Manipulation of equation (7) yields:

$$T = \frac{P}{\rho R} \tag{9}$$

Substituting this and equation (8) into equation (6) yields equation (10):

$$\frac{\gamma}{\gamma - 1}\left[\frac{P_2}{\rho_2} - \frac{P_1}{\rho_1}\right] + \frac{1}{2}\left[v_2^2 - v_1^2\right] = q \tag{10}$$

Rearranging equation (5) we get [4]:

$$P_2 - P_1 = \rho_1 v_1^2 - \rho_2 v_2^2 = \dot{m}\left[v_1 - v_2\right] \tag{11}$$

$$P_2 - P_1 = \rho_1 v_1^2 - \rho_2 v_2^2 = \frac{(\rho_1 v_1)^2}{\rho_1} - \frac{(\rho_2 v_2)^2}{\rho_2} = \dot{m}^2\left[\frac{1}{\rho_1} - \frac{1}{\rho_2}\right]$$

$$\left[v_1 - v_2\right] = \dot{m}\left[\frac{1}{\rho_1} - \frac{1}{\rho_2}\right]$$

$$v_1^2 = \frac{P_2 - P_1}{\rho_1} + \frac{\rho_2 v_2^2}{\rho_1} = \frac{P_2 - P_1}{\rho_1} + \frac{(\rho_2 v_2)^2}{\rho_1 \rho_2}$$

$$v_2^2 = \frac{P_1 - P_2}{\rho_2} + \frac{\rho_1 v_1^2}{\rho_2} = \frac{P_1 - P_2}{\rho_2} + \frac{(\rho_1 v_1)^2}{\rho_1 \rho_2}$$

$$v_1^2 - v_2^2 = \left[\frac{P_2 - P_1}{\rho_1} + \frac{(\dot{m})^2}{\rho_1 \rho_2}\right] - \left[\frac{P_1 - P_2}{\rho_2} + \frac{(\dot{m})^2}{\rho_1 \rho_2}\right]$$

$$v_1^2 - v_2^2 = P_2 - P_1\left[\frac{1}{\rho_1} + \frac{1}{\rho_2}\right]$$

Combining this result with equation (10) yields the Rankine-Hugoniot relation.

$$\frac{\gamma}{\gamma - 1}\left[\frac{P_2}{\rho_2} - \frac{P_1}{\rho_1}\right] - \frac{1}{2}\left[P_2 - P_1\right]\left[\frac{1}{\rho_1} + \frac{1}{\rho_2}\right] = q \qquad (12)$$

The Rankine-Hugoniot curve is shown in Figure 4 below and describes the different possible thermodynamic conditions after a combustion event occurs for the geometry shown in Figure 3. While all of the regions depicted are possible mathematically, not all of them are physically realizable (section V). Analysis of the Rankine-Hugoniot curve shows that there are two possible real combustion processes: those in which pressure and density increase (detonations) and those in which pressure and density decrease (deflagrations). The points at which the Rankine-Hugoniot curve and the Rayleigh lines are tangent are known as the upper (U) and lower (L) Chapman-Jouguet points. These points represent where the post combustion gas velocity is sonic, as dictated by the Rayleigh limit for heat addition in a constant area tube.

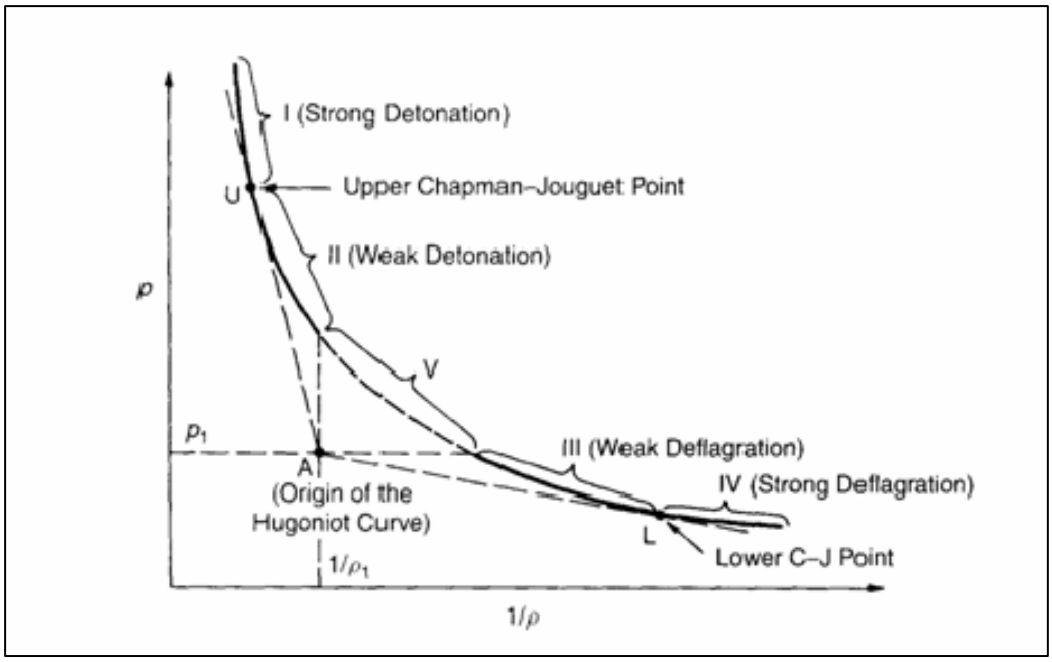

Figure 4. Hugonoit curve on *P*-versus-*1/p* plane (from [2])

C. DETONATION INITIATION AND PROPAGATION

Three methods can be utilized to achieve a detonation in fuel air mixtures. A detonation can be directly produced through the use of a high energy ignition source or it can be indirectly produced through a process called Deflagration to Detonation Transition (DDT). A third method exists, SDT – shock induced detonation; however, this method is not commonly used.

Directly detonating a fuel air mixture requires enormous amounts of energy, in excess of 1000 Joules, and is often achieved through the use of high explosives. Alternatively, the circuitry and energy source required for generating such high voltage high amperage discharges are heavy and bulky. Utilizing either approach on a PDE designed for an airborne application is not a viable option. Another option for the direct detonation of fuel air mixtures involves the utilization of an "initiator" which uses a highly detonable fuel/oxygen mixture to generate a strong denotation and propagate a shock wave from one mixture to another less sensitive mixture in a combustor. This generally results in a detonation in the main combustor. The main combustor contains a

less detonable mixture such as ethylene/air or JP-10/air. However, it was found that the gain in detonability is offset by a reduction in specific impulse (I_{sp}) since the auxiliary fuel/oxygen mixture used in the "initiator" must be considered as a "fuel" for I_{sp} calculations. As seen from Equation (13), I_{sp} will decrease for a given thrust level as mass flow rate of fuel and/or required initiator reactants increases.

$$I_{sp} = \frac{Thrust}{\dot{m}_{fuel} + \dot{m}_{init}} \tag{13}$$

DDT is the other method commonly used to produce a detonation and it is explained well by Kuo where he summarizes the transition in the following steps [2]:

1. Generation of compression waves ahead of an accelerating laminar flame (see Figure 5). The laminar flame front is wrinkled at this stage.
2. Formation of a shock front due to coalescence of compression waves (see Figure 5).
3. Movement of gases induced by the shock, causing the flame to break into a turbulent brush (see Figure 5).

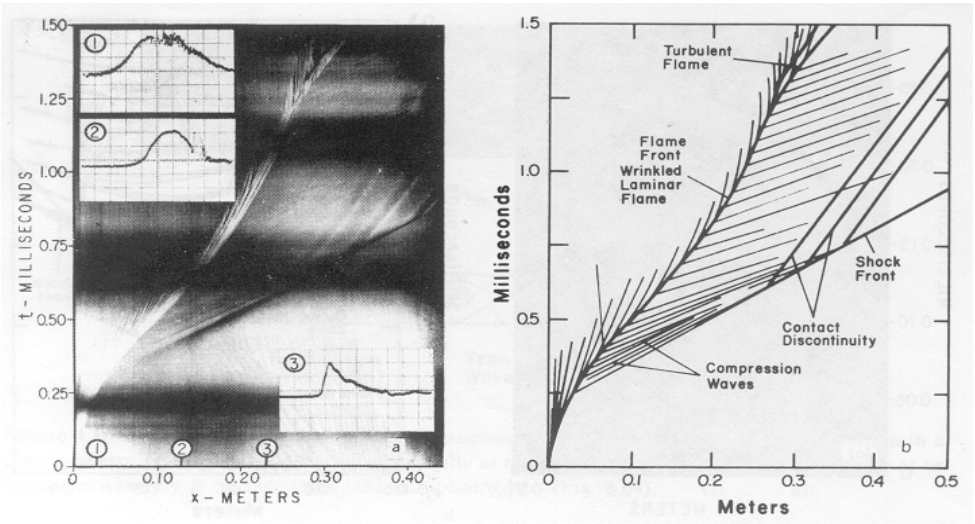

Figure 5. Streak schlieren photograph of the development of detonation (from [2])

4. Onset of “an explosion in an explosion” at a point within the turbulent reaction zone, producing two strong shock waves in opposite directions and transverse oscillations in between. These oscillations are called transverse waves (see Figure 6). The forward shock is referred to as super-detonation and moves into the unburned gases. In the opposite direction, a shock moves into the burned gases and is know as retonation.

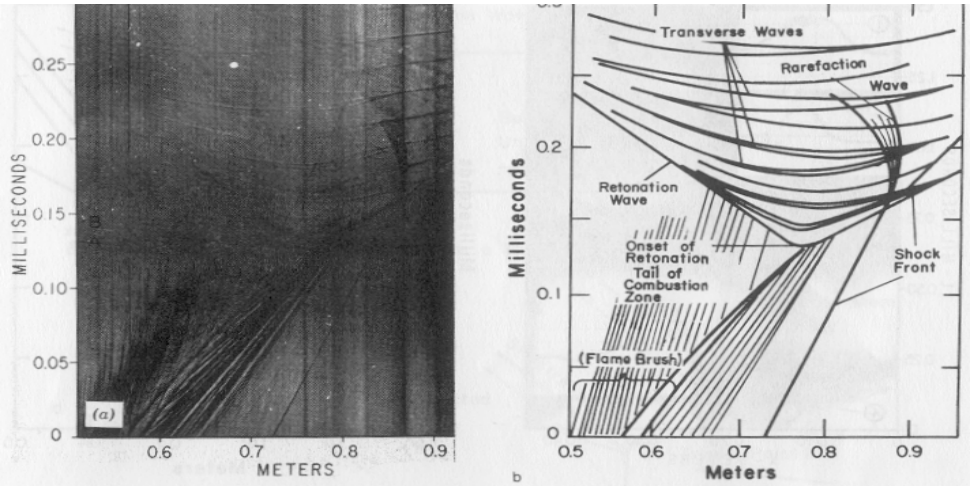

Figure 6. Streak schlieren photograph of the onset of retonation (from [2])

5. Development of spherical shock waves at the onset of the “explosion in an explosion” with a center located in the vicinity of the boundary layer (see Figure 7).

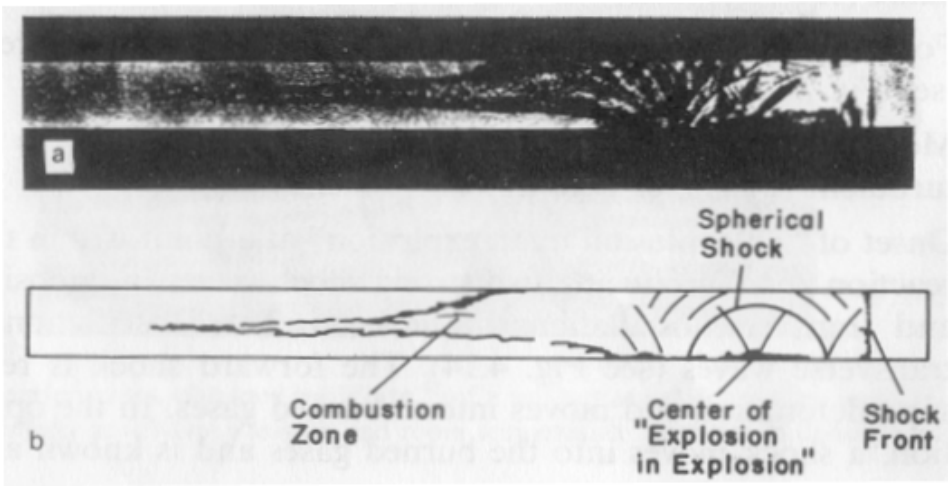

Figure 7. Flash schlieren photograph of the onset of retonation (from [2])

6. Interaction of transverse waves with shock front, retonation wave, and reaction zone (see Figure 8).
7. Establishment of a final "steady wave" as a result of a long sequence of wave interaction processes that lead finally to the shock deflagration ensemble: the self-sustained C-J detonation.

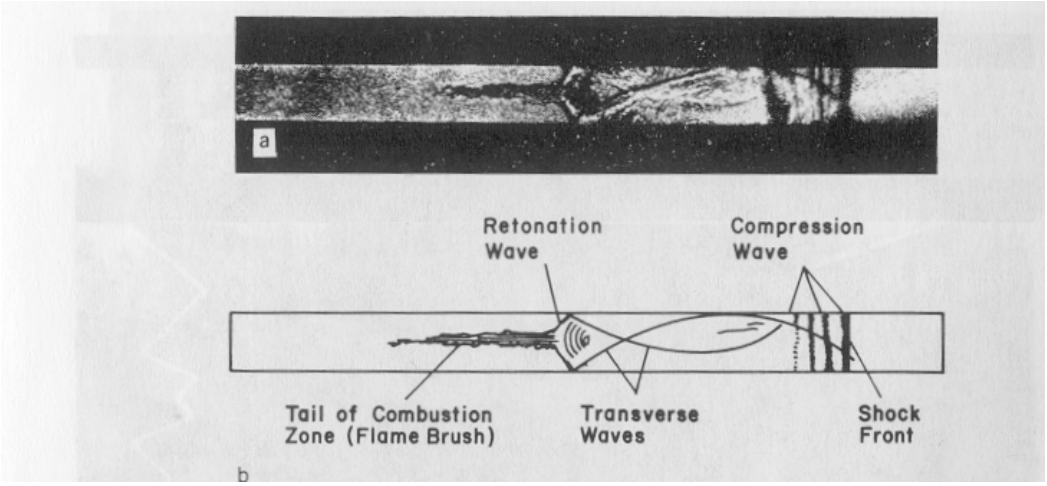

Figure 8. Flash schlieren photograph of transverse waves set up at the onset of retonation (from [2])

Experimentation in the 1960s revealed a commonality of structure shared by all detonation events. Original models of the detonation wave assumed a one dimensional structure, known as the 1-D Zeldovich–Neumann–Döring (ZND) detonation wave. An example is shown below in Figure 9. Moving from right to left the model illustrates the property changes that occur during a detonation event. Across the leading shock wave the reactants increase in pressure and temperature due to compression heating. Following the shock wave is a large deflagration zone, where most of the reactions, and therefore heat release, are believed to occur. The deflagration zone consists of two separate zones called the induction zone and the reaction zone. In the induction zone it is assumed that minimal reactions occur for a short period of time after the shock wave. Since the thickness of the shock wave is only on the order of two to three molecular mean free path lengths, the shocked molecules are typically excited in their vibrational degrees of freedom and are in local non-equilibrium states. After some time, typically tens of microseconds, energy equipartition occurs which transfers energy among the kinetic

degrees of freedom. It is at this time, after the relaxation process occurs that the molecules start to heavily interact with their neighbors and chemical reactions take off. In the reaction zone following the induction zone, the reaction rate increases to an extremely high value resulting in a rapid increase in temperature and a subsequent decrease in pressure and density. Following completion of the reaction, the properties relax to near equilibrium values.

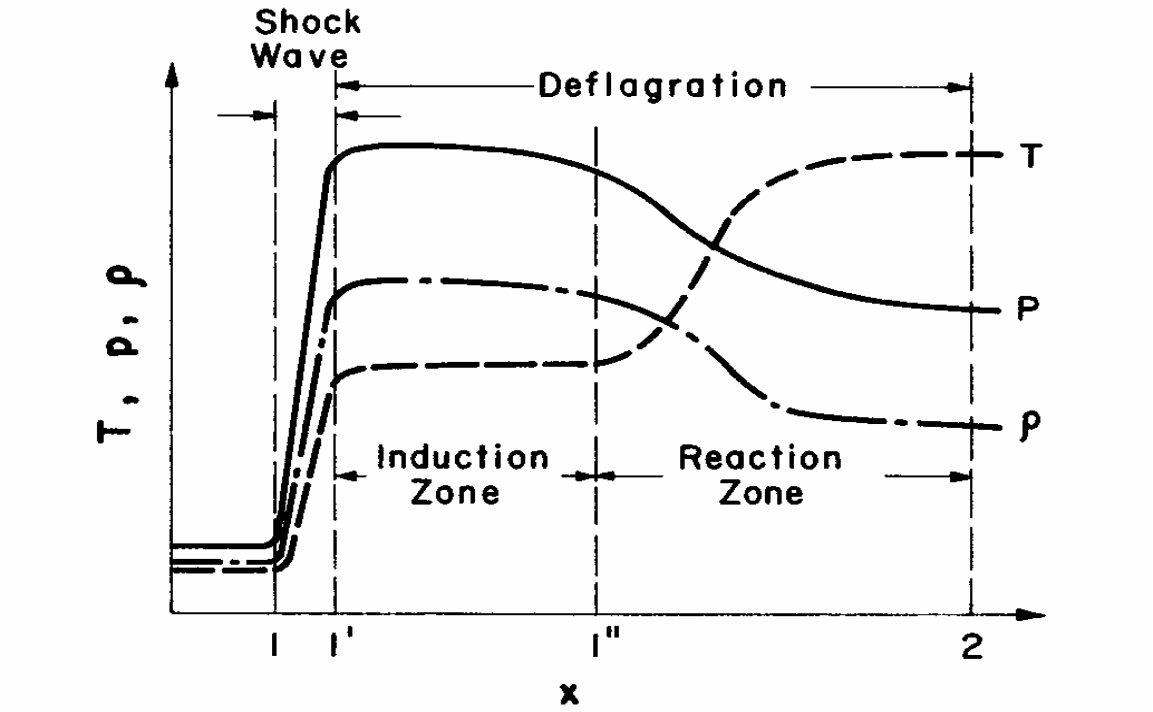

Figure 9. Variation of physical properties through a ZND detonation wave (from [2])

In the early 1900s scientists realized that there was also a three dimensional structure to detonation waves. Kuo characterizes the 3-D detonation as follows [2]:

> The detonation-wave structure is characterized by a non-planar leading shock wave which at every instant consists of many curved shock sections which are convex toward the incoming flow. The lines of intersection of these curved shock segments are propagating in various directions at high velocities (see Figure 10).

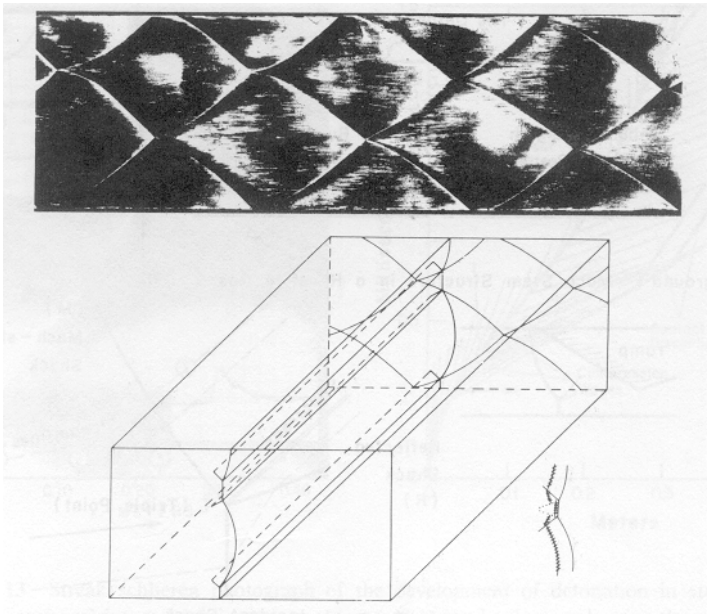

Figure 10. Smoked-foil record and schematic diagram of symmetric planar interaction (from [2])

The third shock, R, (see Figure 11) of these intersections extends back into the reactive flow regime and is required for the flow to be balanced at the intersection of the two convex leading shock waves. In general, the flow in the neighborhood of the shock front is quite complex. The schematic diagram of symmetric planar interaction is shown in Figure 11.

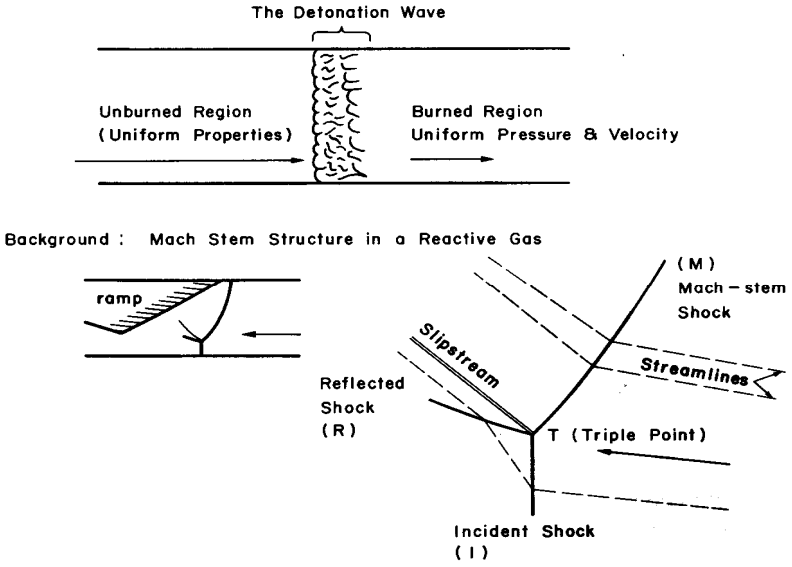

Figure 11. Shock-wave pattern and triple point in a two-dimensional supersonic flow passing through a convergent ramp section (from [2])

The detonation is the fundamental process which enables the operation of the PDE. Having discussed the structure of a detonation and how it is initiated, we can now explore the thermodynamic advantages of utilizing the process in an operational PDE.

D. PDE THERMODYNAMIC CYCLE

Analysis has been performed comparing the theoretical performance of a detonation combustion cycle to that of the Brayton cycle using ethylene and air as the reactants. The PDE cycle is different from the Brayton cycle because it detonates the fuel air mixture vs. the deflagration that occurs in the Brayton cycle. That detonation results in a rapid increase in temperature and pressure at a nearly constant volume, while the deflagration results in an increase in temperature at a constant pressure. Due to the increase in both temperature and pressure, the constant volume PDE cycle is more thermodynamically efficient than the constant pressure Brayton cycle.

$$\eta_{th} = \frac{W_{net}}{q_{in}} \tag{14}$$

Using CEQUEL, a comparative analysis of the PDE and Brayton cycles was performed at a flight Mach number of 4. Identical inlet losses and MIL-SPEC conditions where assumed for the analysis. Both cycles utilized an ethylene fuel-air mixture with an equivalence ratio of one. For both Figure 12 and 13, the process occurring from points 1 to 2 represents the combustion event, and the process from points 2 to 3 represents the combustion products expanding isentropically to ambient pressure. From points 3 to 4 the remaining heat is rejected to the atmosphere at constant pressure. The final stage from points 4 to 1 represent the compression ratio due to the supersonic flight Mach number and the MIL-E_5007D inlet recovery factor.

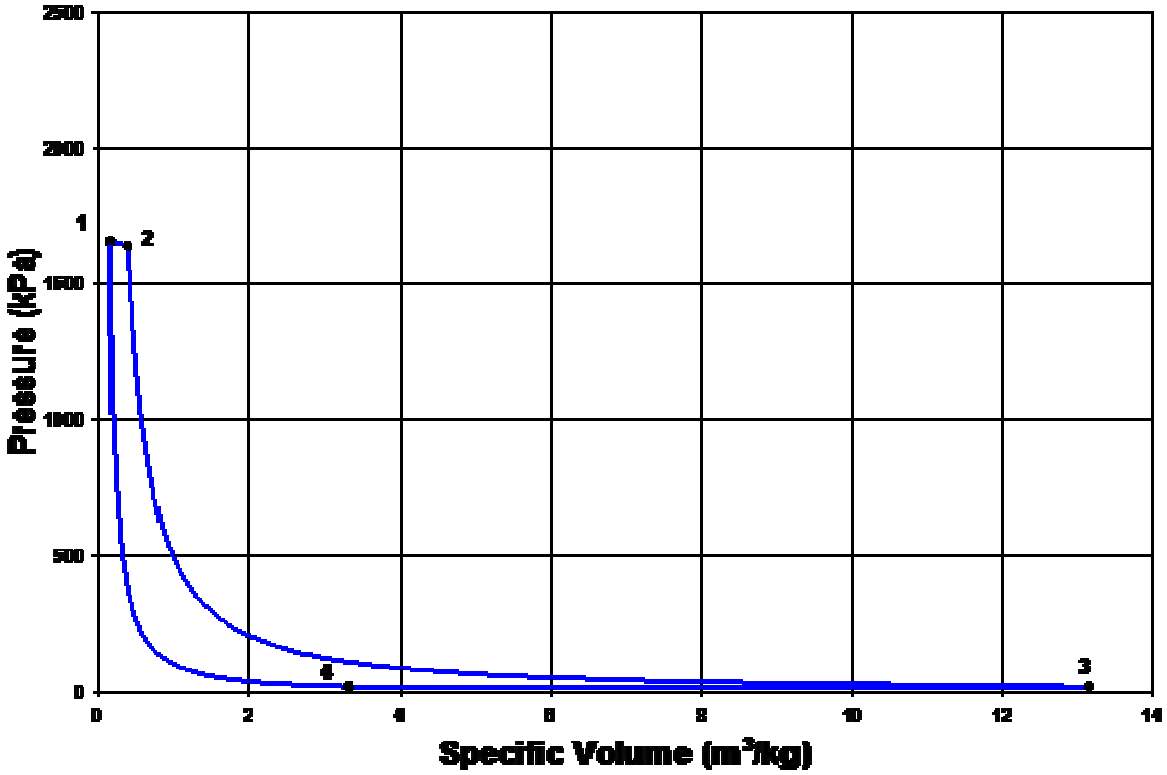

Figure 12. P-V for a Brayton Cycle at Mach 4

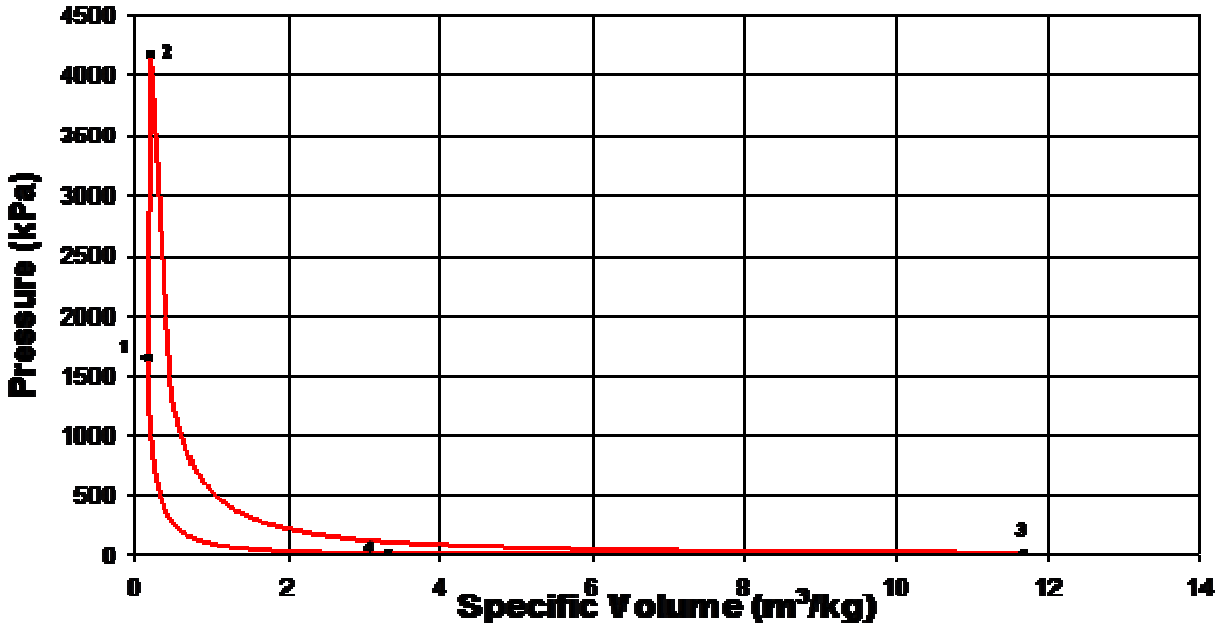

Figure 13. P-V diagram for a PDE at Mach 4

The work performed by each cycle can be determined by integrating the area under the curve from points 2 to 3, and then subtracting the integrated area under the curve from points 3 to 1.

$$w_{PDE} = \int_2^3 p\,dv - \int_4^1 p\,dv - p_4(v_3 - v_4) = \frac{p_1 v_1 - p_4 v_4}{1-\gamma} + \frac{1}{2}\left(\frac{p_2 - p_1}{v_2 - v_1}\right)\left(v_2^2 - v_1^2\right) + \left[p_2 - \left(\frac{p_2 - p_1}{v_2 - v_1}\right)v_2\right](v_2 - v_1) + \frac{p_3 v_3 - p_2 v_2}{1-\gamma} + p_3(v_4 - v_3) \tag{15}$$

$$\begin{aligned} w_{Brayton} &= p_1(v_2 - v_1) + \int_2^3 p\,dv - \int_4^1 p\,dv - p_4(v_3 - v_4) \\ &= p_4(v_4 - v_3) + \frac{(p_1 v_1 - p_4 v_4)}{1-\gamma} + \frac{(p_3 v_3 - p_2 v_2)}{1-\gamma} + p_1(v_2 - v_1) \end{aligned} \tag{16}$$

Using the properties from tables 3 and 4 and equation (13) the net work and thermal efficiency for each cycle can be calculated. Based on the results shown below in table 5, the PDE clearly outperforms the Brayton cycle at this Mach number both in terms of net work and cycle efficiency.

Table 3. Brayton cycle properties at M=4

Brayton					
	T(k)	**P**(kPa)	**Gamma**	**S**(J/K)	**V** (m^3/kg)
1	892.6	1657.14	1.39	162.01	0.154
2	2211.8	1639.48	1.24	1510.59	0.387
3	859.3	18.75	1.27	1510.57	13.2
4	216.7	18.75	1.39	0	3.32

Table 4. PDE cycle properties at M=4

PDE Cycle					
	T(k)	**P**(kPa)	**Gamma**	**S**(J/K)	**v** (m^3/kg)
1	892.7	1639.7	1.39	165.04	0.156
2	2829.7	4185.5	1.30	1349.6	0.194
3	762.7	18.7	1.32	1349.6	11.677
4	216.7	18.7	1.39	0	3.32

Table 5. Brayton-PDE cycle comparison

	Net Work (kJ/kg)	η (%)
PDE	1803	57.1
Ramjet	1092	37.3

E. PDE PERFORMANCE

The higher thermodynamic efficiency in the PDE cycle has been demonstrated; however the cycle is an unsteady one, which creates additional challenges. In order for the advantages of the cycle to be realized, the discrete impulses produced by each detonation must be repeated at high frequencies to produce a near steady thrust. High frequency operation requires that each step in the cycle shown in Figure 1 be optimized to reduce total cycle time and therefore increase the potential operating frequency of the engine. The total time for one cycle and each of the individual processes in the cycle can be represented by the following equations.

$$t_{\text{cycle}} = t_{\text{fill/refresh}} + t_{\text{ignition-delay}} + t_{\text{ddt}} + t_{\text{detonation}} + t_{\text{blowdown/purge}} \tag{17}$$

$$t_{fill/refresh} = \frac{l_{initiator}}{M_{fill/refresh} c} \tag{18}$$

$$t_{ddt} = t_{ignDelay} + 500\mu s \tag{19}$$

$$t_{\text{detonation}} = \frac{l_{\text{remaining}}}{M_{\text{det}} c} \tag{20}$$

Ignition delay, $t_{\text{ignition-delay}}$, is the time required for the ignition event to become a fully developed flame. Experimental results indicate that it is on the order of 2 ms for the transient plasma ignition device currently in use on the Naval Postgraduate School PDE. Purge and blow down time, $t_{\text{blowdown/purge}}$, is the amount of time required to flush the hot products from the engine prior to new reactants entering. This time is design dependant and can be reduced by minimizing recirculation areas in the engine, or by decreasing

blow down time. Recirculation areas tend to retain hot combustion products, similar to a flame holder in a ramjet, and can pre-ignite an incoming fuel air mixture.

The initiator length, $l_{\text{initiator}}$, is broken into two sections in equations 19 and 20; the length required for the deflagration to detonation process to occur and the length remaining after detonation formation. It is clear from equations 18 and 20 that by reducing the length of the initiator, and therefore the length remaining after DDT, we can reduce the cycle time. However, retaining a constant diameter, a decrease in the length of the initiator will also result in a decrease in the volume of fuel and air detonated per cycle, therefore reducing thrust. Increasing the diameter of the initiator tube will increase the volume of the initiator for a given length, and will also allow for a larger mass flow of reactants through the engine; however the diameter is limited to that necessary to support a three dimensional detonation wave structure, which is near one cell size [4].

Increasing mass flow rate through the engine will reduce $t_{\text{fill/refresh}}$ as shown in equation 21. Mass flow can be increased until the flow becomes choked, however at some point the increased pressure drop in the engine associated with the higher fluid velocity may outweigh the advantages of operating at a higher frequency. Additionally high flow speeds in the initiator can prevent ignition of the fuel air mixture.

$$M_{\text{fill/refresh}} = \frac{\dot{m}}{\rho_{\text{refresh}} A_{\text{initiator}} \sqrt{\gamma RT}} \qquad (21)$$

Clearly a balance must be struck between initiator length, diameter and mass flow rate to achieve maximum operating frequency, and therefore the maximum thrust, available. Consideration of the practical application of the PDE when it is put into service will likely influence how the PDE is optimized for each platform.

Another method of varying the thrust produced by the engine is by changing the fill fraction, or the amount of fuel added to the engine per cycle. This can be accomplished simply by increasing the delay before the fuel injectors are turned on and thereby reducing the amount of time the fuel injector is open per cycle, therefore keeping a near constant mixture over a shorter axial length and reducing the overall fuel to air ratio (f). This is commonly referred to as a partial fill scenario.

$$f = \frac{\dot{m}_{fuel}}{\dot{m}_{air}} \tag{22}$$

$$thrust = \dot{m}_{air}((1+f)u_{exit} - u_{inlet}) \tag{23}$$

$$\phi = \frac{f}{f_{stoichiometric}} \quad = \text{Equivalence Ratio} \tag{24}$$

Equivalence ratio is a term widely used to describe the composition of a mixture used in combustion events. The equivalence ratio, ϕ, is defined as the fuel-to-oxidizer mass ratio of reactants, divided by the stoichiometric mass ratio of fuel-to-oxidizer reactants; as shown in equation 24. The effects of ϕ on the pressure change across a detonation wave and detonation wave velocity were calculated using CEQUEL and are shown in Figures 14 and 15 below.

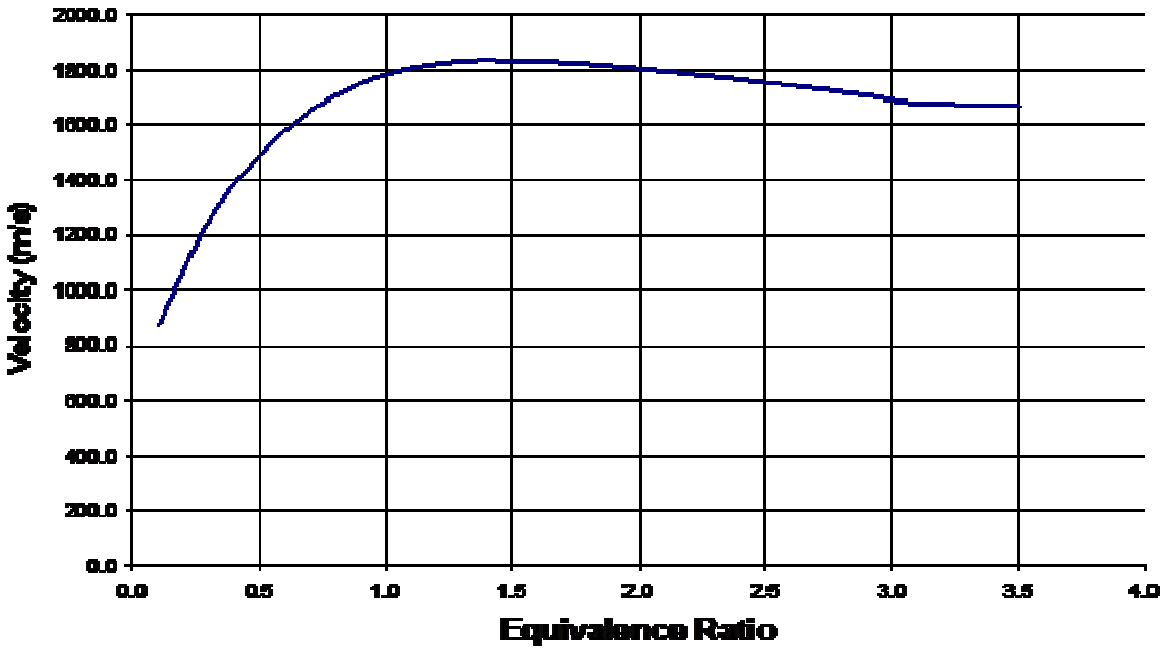

Figure 14. Velocity vs. equivalence ratio for an ethylene-air detonation

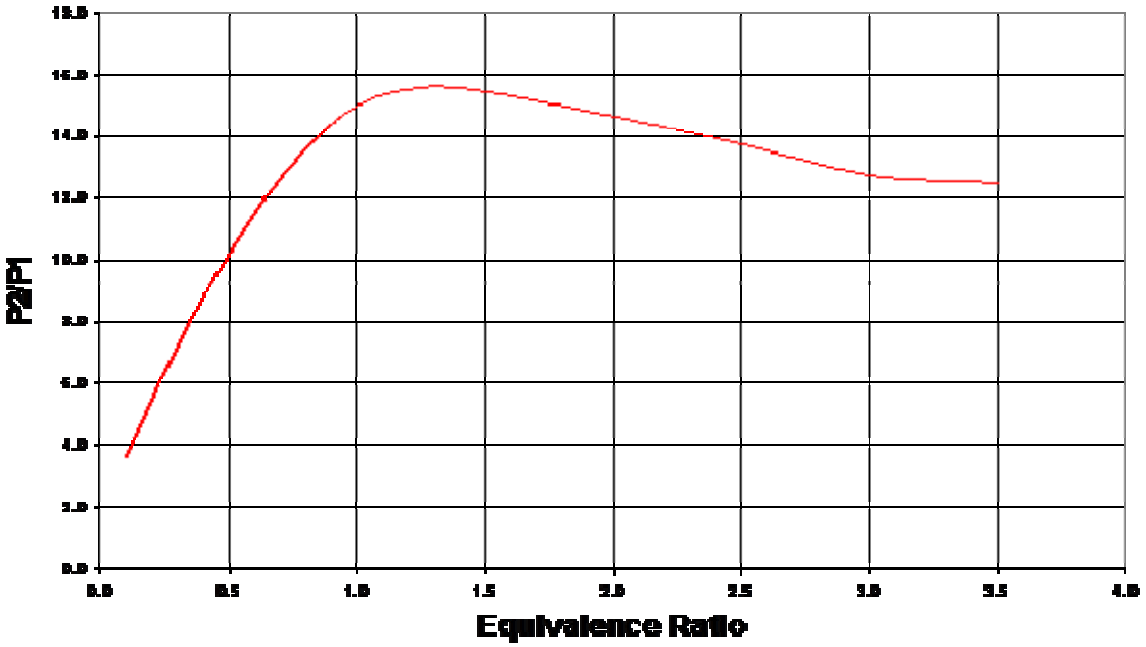

Figure 15. Pressure ratio vs. equivalence ratio for an ethylene-air detonation

III. MODELING AND DESIGN

A. CFD ANALYSIS

Fluid flow through various inlet orifice geometries was performed using a software package developed by Computational Fluid Dynamics Research Corporation (CFDRC) and sold by the ESI Group. The software package consists of four separate computational programs; CFD-GEOM, CFD-ACE, CFD-FASTRAN and CFD-VIEW. CFD-GEOM is the program used to construct the geometry and mesh for the desired model. Axis-symmetric models were used in most cases due to computational constraints, with the lower boundary of the model representing the axis. Two dimensional models were constructed to simulate the inlet arms of the PDE, were dimensionally accurate, and extended downstream to the ethylene fuel injector location shown in Figures 16 and 17. Boundary conditions for all models included a symmetry boundary (as applicable), an inlet and an outlet, and wall boundaries.

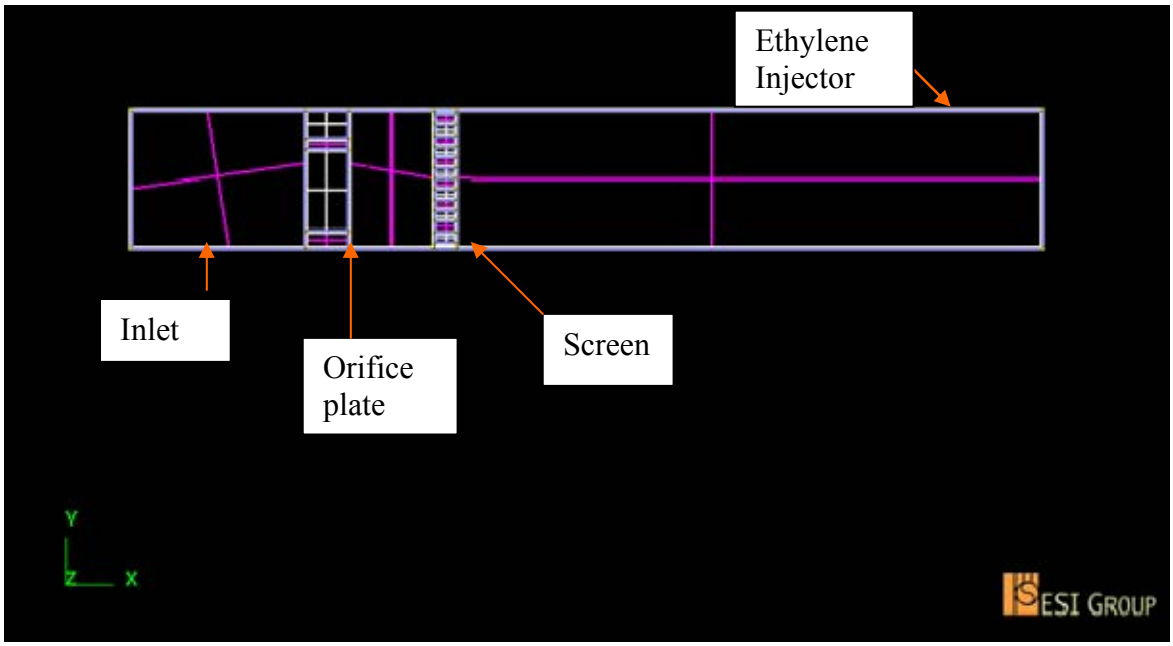

Figure 16. CFD-GEOM model of PDE inlet arm orifice plate and screen

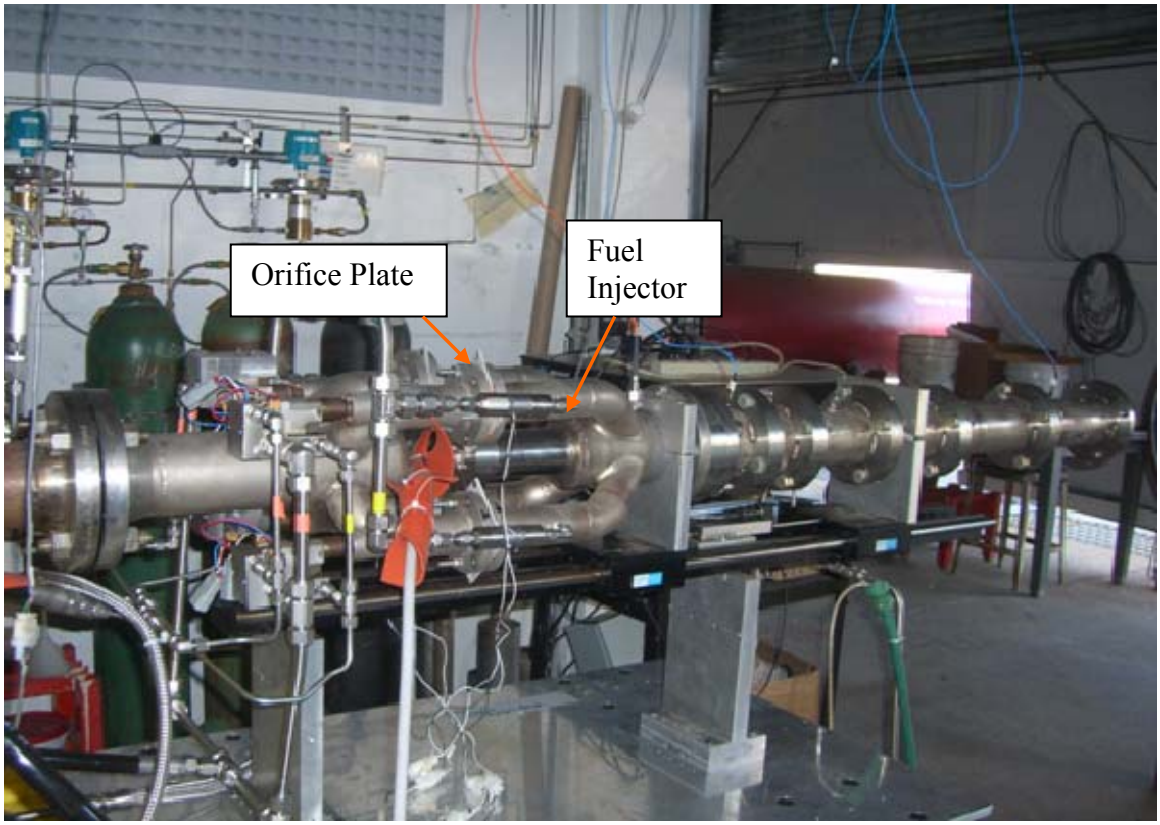

Figure 17. PDE orifice plate and injector locations

After the models were constructed using CFD-GEOM they were exported to a .DTF file and then imported into CFD-FASTRAN. CFD-FASTRAN uses a density based compressible Euler and Navier-Stokes differential equation flow solver that allows numerical solutions of subsonic, sonic and supersonic flow fields. It employs state-of-the-art turbulence models for predicting the effects of turbulence within boundary layers and separation regions [14, 15].

Steady state simulations were performed on all models using inlet pressures of four, eight and sixteen atmospheres exhausting to one atmosphere. These settings were based on observed values during engine operations at various flow rates. Three of the models evaluated, with velocity profiles, are shown in Figures 18 through 23. In each case the pressure differential across the plate was eight atmospheres and velocity profiles were taken three inches downstream of the orifice plate or screen, as applicable.

B. COMPUTATIONAL RESULTS

Analysis was first performed on the existing single orifice design. As seen in Figures 18 and 19 below significant fluid recirculation zones extended for several inches downstream of the injector location.

A number of different single orifice designs were evaluated, including convergent-divergent nozzles, convergent-divergent nozzles with discrete steps in the divergent portion, and simple orifices with divergent outlets. Similar to the simple orifice, each of these design iterations displayed significant downstream recirculation zones, and were therefore eliminated as possible solutions.

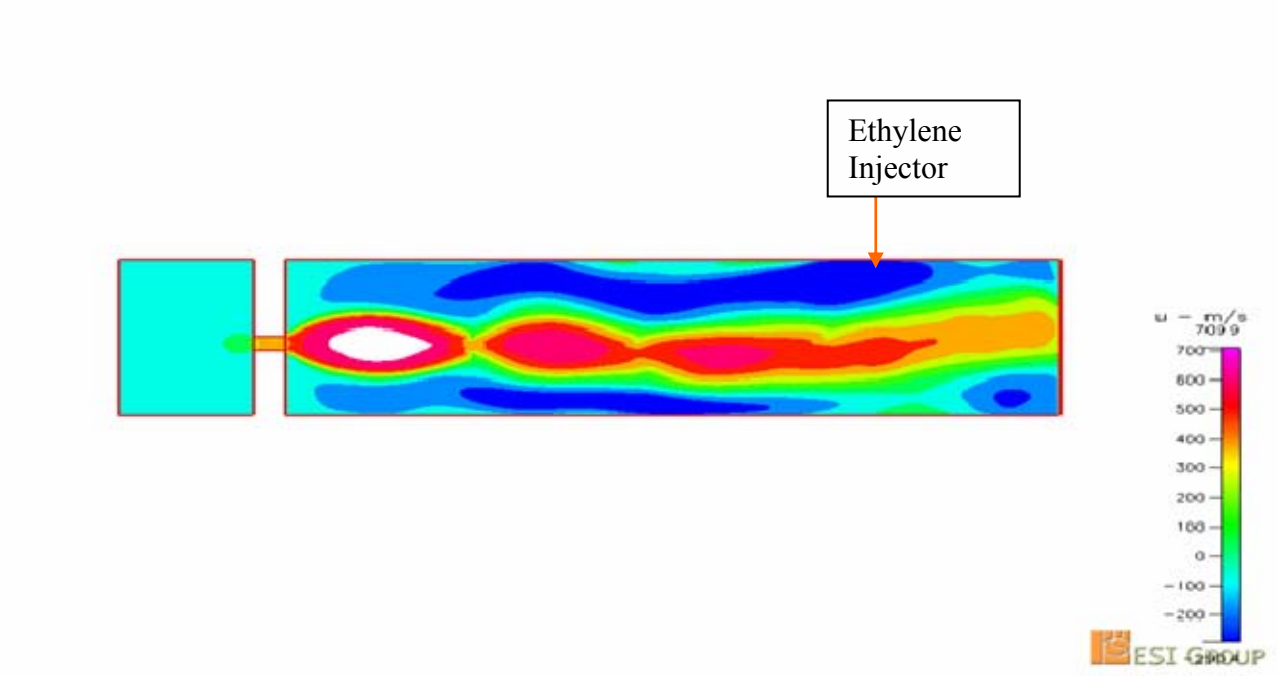

Figure 18. Single Orifice CFD results

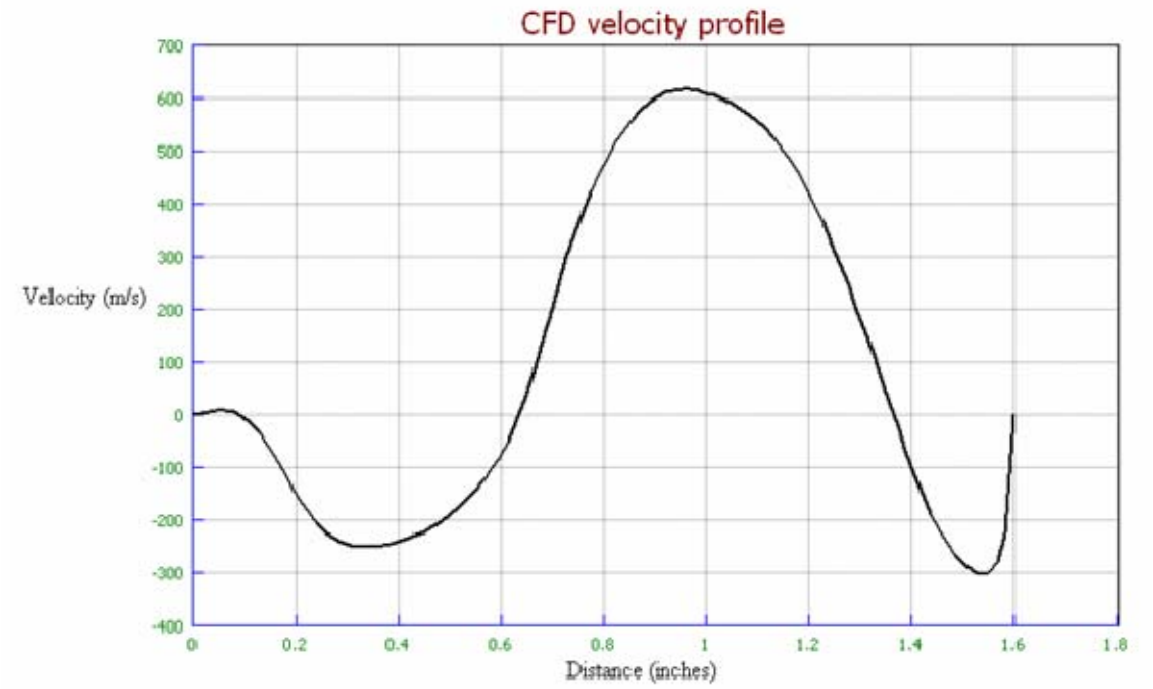

Figure 19. CFD fluid velocity profile for single orifice

Due to the lack of success with the single orifice design the next iteration implemented multiple orifices consisting of a single, larger orifice in the center and several smaller orifices around it. Care was taken to ensure the total flow area through the multiple orifice plate did not change when compared to the single orifice design. Outer orifice location and number was determined through multiple iterations of the design in an effort to minimize downstream recirculation zones. This design showed significant improvement over the single orifice design, however small recirculation zones continued to form downstream of the orifice plate. In an effort to reduce the size of the recirculation zones further a 1/16" flow conditioning screen was added one half inch downstream of the orifice plate. Results from each of these configurations can be seen in Figures 22 and 23. The flow conditioning screen largely eliminated bulk recirculation zones and, combined with the multiple orifice design, had the effect of flattening out the velocity profile downstream.

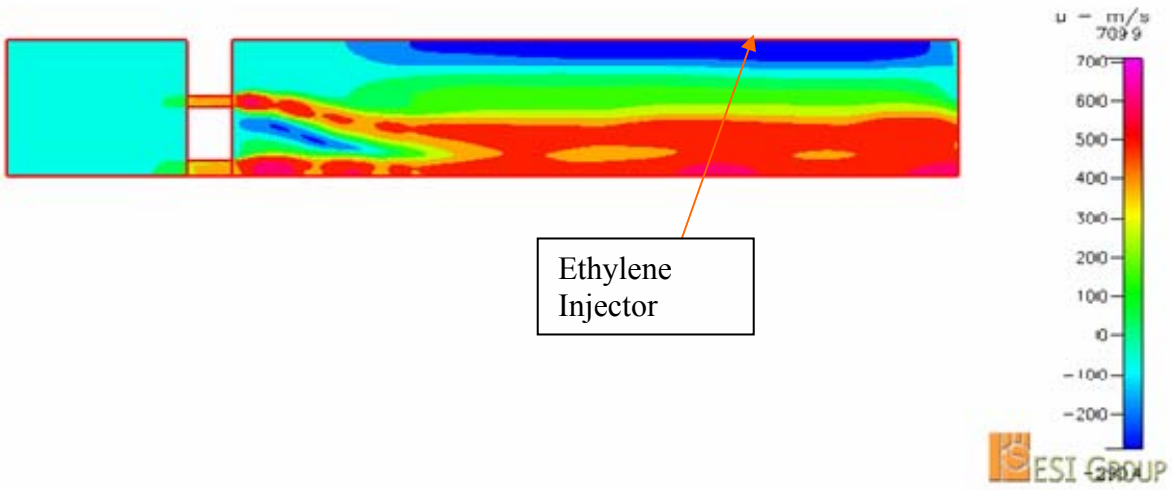

Figure 20. Axis-symmetric multiple orifice CFD results

Figure 21. CFD fluid velocity profile for multiple orifice plate (Axis-symmetric)

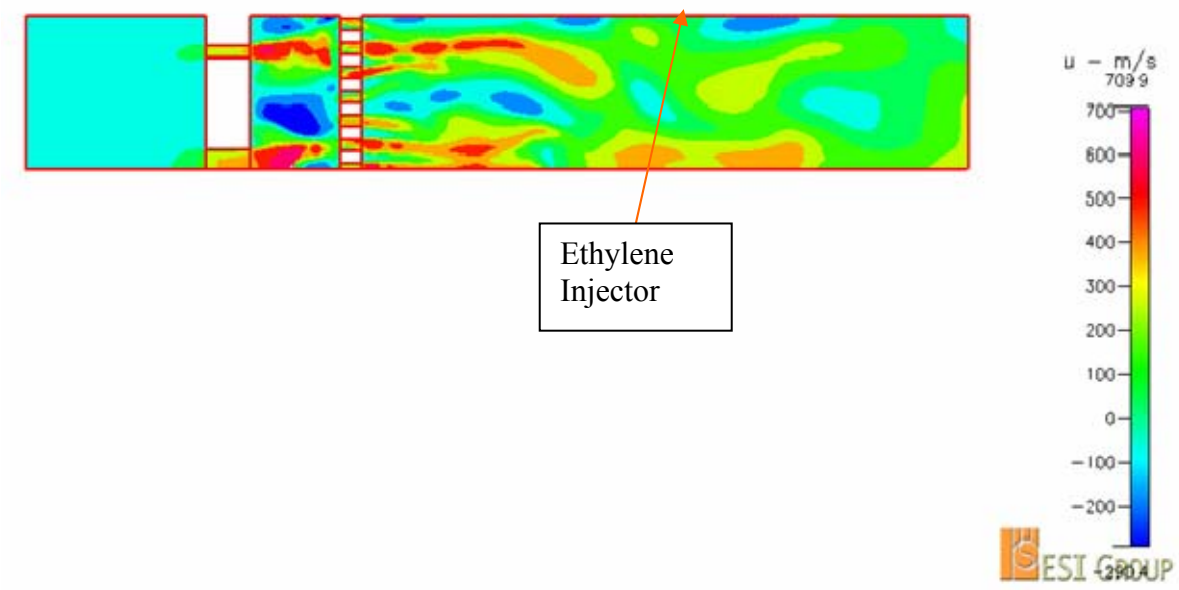

Figure 22. CFD results for multiple orifice plate with screen (Axis-Symmetric)

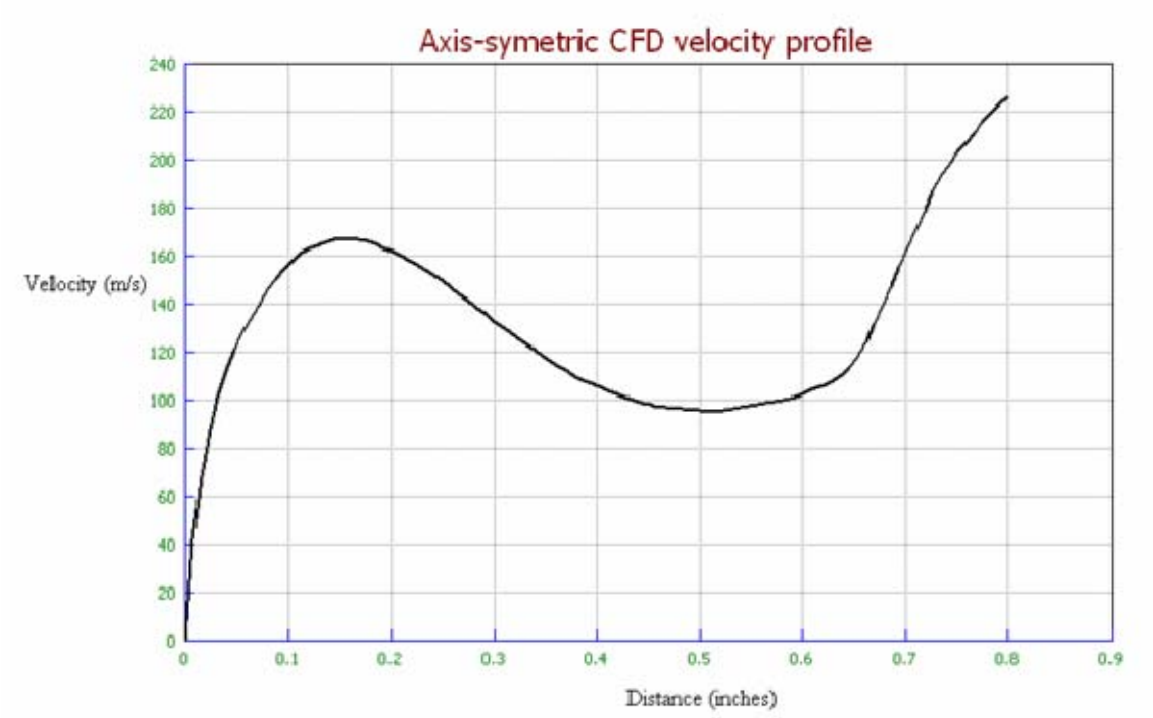

Figure 23. CFD fluid velocity profile, multiple orifice with screen

C. MULTIPLE ORIFICE / SCREEN PLATE DESIGN

Based on the results from CFD orifice and screen plates were designed using a three dimensional computer aided design software package named Autodesk Inventor. Both plates were machined from stainless steel and are shown in Figure 24 below. Detailed orifice and screen plate design specifications are included in Appendix A.

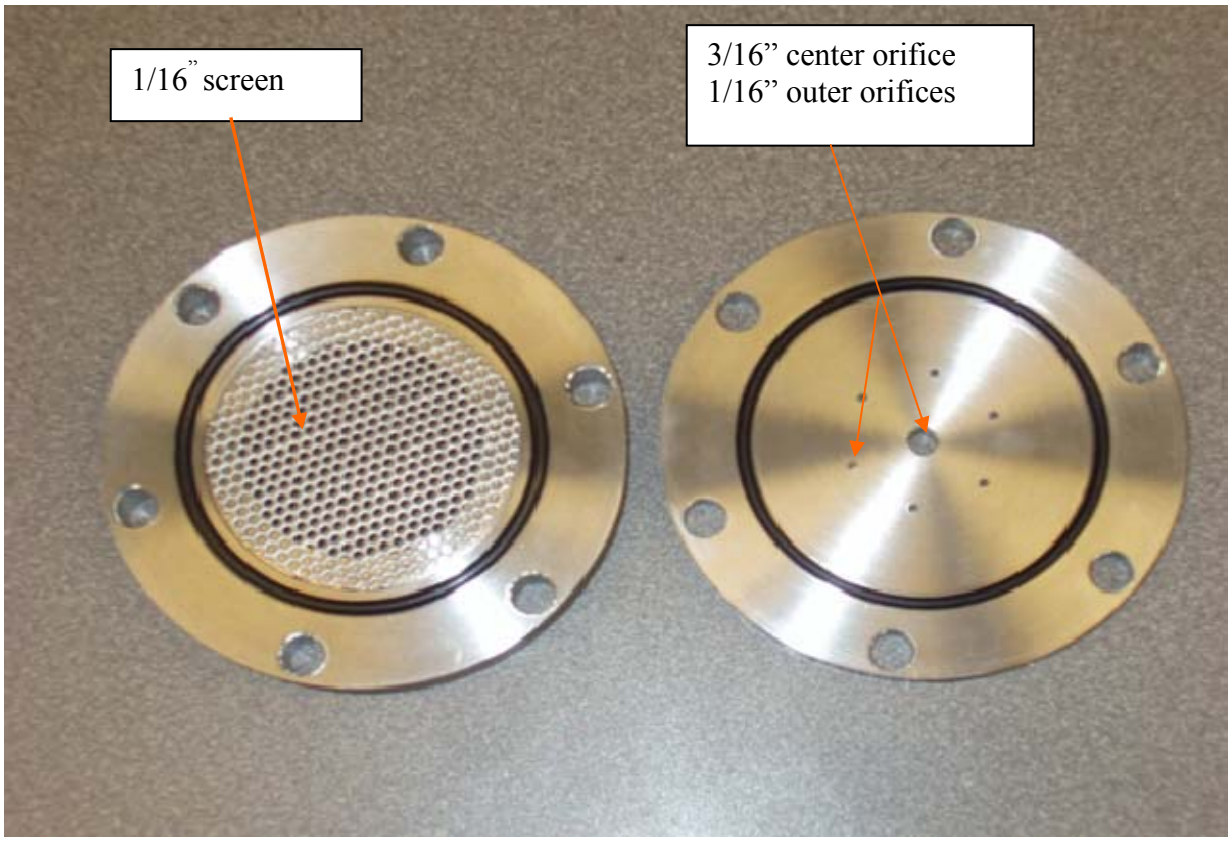

Figure 24. Orifice and screen plates

THIS PAGE INTENTIONALLY LEFT BLANK

IV. EXPERIMENTAL SETUP

A. PDE

For the purposes of this experiment air flow was delivered to the PDE at 0.25kg/s, 0.31 kg/s and 0.35 kg/s. The air was heated by a hydrogen/oxygen vitiator at the inlet of the PDE to simulate the temperatures/pressures produced by inlet compression at high speed flight conditions, and fuel was injected at various pressures. A test matrix for JP10-air and Ethylene-Air is shown below in Table 6.

Table 6. JP10/Ethylene-Air test matrix

Air Flow rate	Ethylene Pressure (MPA)				
	2.41	2.75	3.09	3.43	3.78
.25 kg/s	X	X	X		
.31 kg/s		X	X	X	
.35kg/s			X	X	X
	JP10 (Oil Pressure MPA)				
	3.79	8.48			
.31kg/s	X	X			

Figure 25. Hydrogen/Oxygen Vitiator

The ethylene injectors were electronically actuated, with ethylene pressure controlled by a pressure regulator located upstream of the injector. Due to the rapid, highly transient nature of the injection event ethylene pressure was used for the purposes of this experimentation vs. the manufacture's provided valve flow rates, which are based on steady state flow conditions.

JP10 is injected using an elctro-hydraulically actuated piston type injector assembly. They inject a constant volume of 130 mm^3 of fuel with the injection rate controlled by varying the actuating oil pressure.

B. LASER DIAGNOSTICS

The fuel profile was obtained through transmission measurements by mounting a 3.39 μm Helium Neon laser immediately downstream of the PDE exit plane. The laser was directed across the exit plane, through a chopper wheel operating at 440 kHz and into a +/-10 volt dynamic IR receiver.

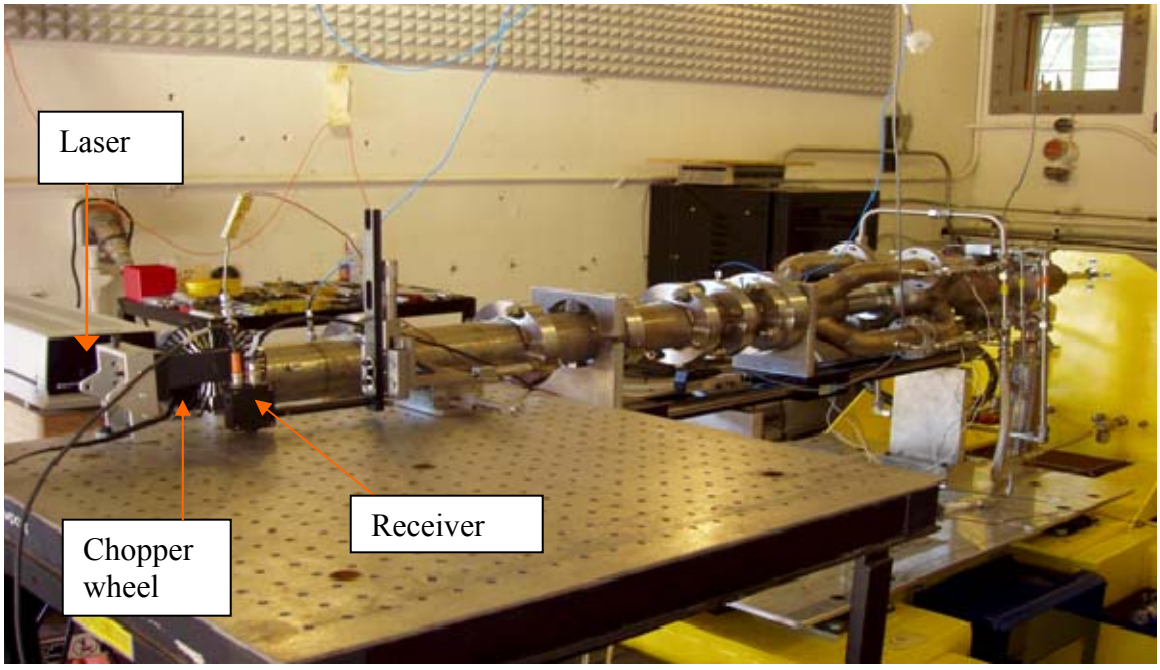

Figure 26. Helium-Neon laser with receiver and chopper wheel

Voltage output from the receiver was proportional to the intensity of the light entering, however because it was a dynamic receiver the use of a chopper wheel was required. The purpose of the chopper wheel was to interrupt the optical output of the laser at discrete intervals therefore providing a dynamic input to the receiver. The effect was a nearly sinusoidal voltage output across a preset voltage band as shown in Figure 27.

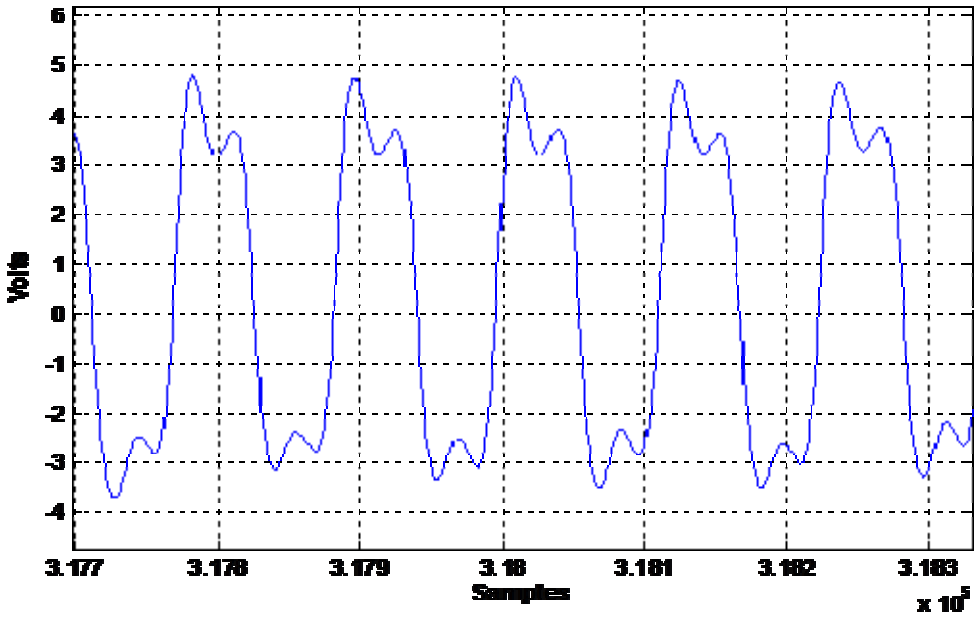

Figure 27. Laser receiver output to data acquisition unit

By determining the minimum and maximum values of the voltage output laser intensity can be determined. As shown in Figure 28, as the fuel plug passes through the laser beam some of the light is absorbed by the fuel, resulting in a decrease in the difference between the maximum and minimum voltages. This absorption can be described by the Beer-Lambert law, shown in equation 25, where I is in transmitted voltage difference, Io is the baseline voltage difference, σ_v is the absorption cross section of the absorbing species, N is molar density of the absorbing species and L is the transmission path length of the sample.

$$\frac{I}{I_0} = e^{-\sigma_v NL} \qquad (25)$$

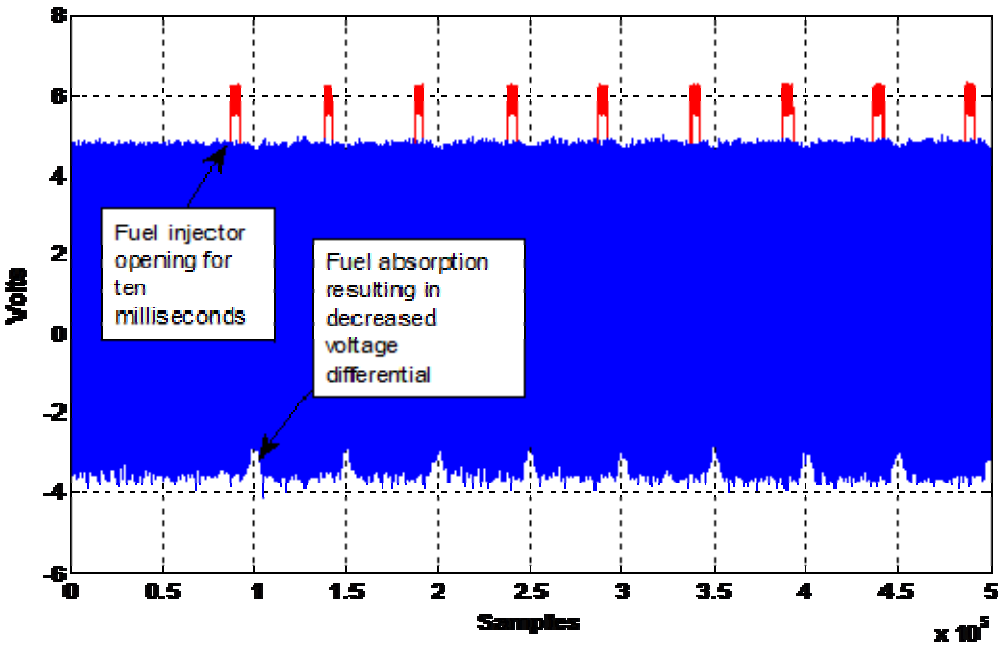

Figure 28. Raw Data from 10Hz ethylene injection

Using the ideal gas law this equation can be rearranged to solve for the mole fraction of the absorbing species as follows [6]:

$$X_i = \frac{-\ln(\frac{I}{I_0})RT}{\sigma_v PL} \qquad (26)$$

In this equation R is the universal gas constant, T is the temperature in degrees Kelvin, P is the static pressure and X_i is the molar fraction of the absorbing species. Absorption cross sections for ethylene and JP10 at 3.39 μm were provided by Stanford University and are included as Figures 29 and 30.

Once molar fraction of the absorbing species was found mass fraction was calculated using the following equation, where M is the molecular weight of the given substance.

$$\frac{X_{i(species)}}{(1-X_i)_{(air)}} * \frac{M_{species}}{M_{air}} \qquad (27)$$

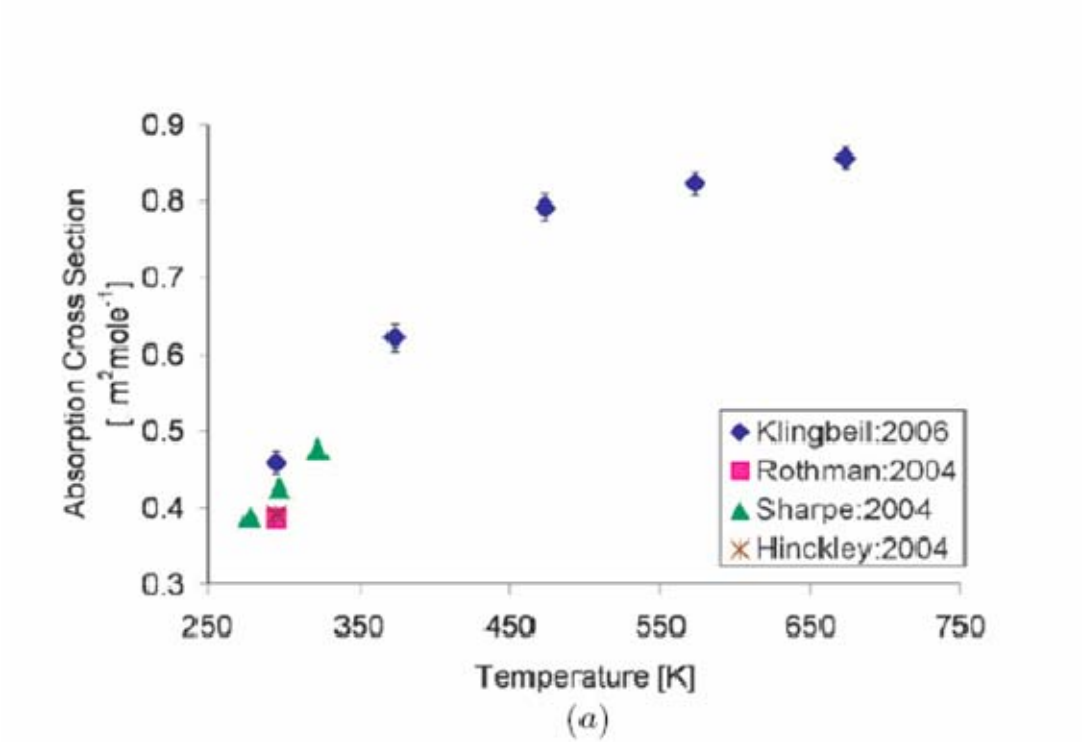

Figure 29. Absorption cross section of ethylene at 1 atm. as a function of temperature (from [6])

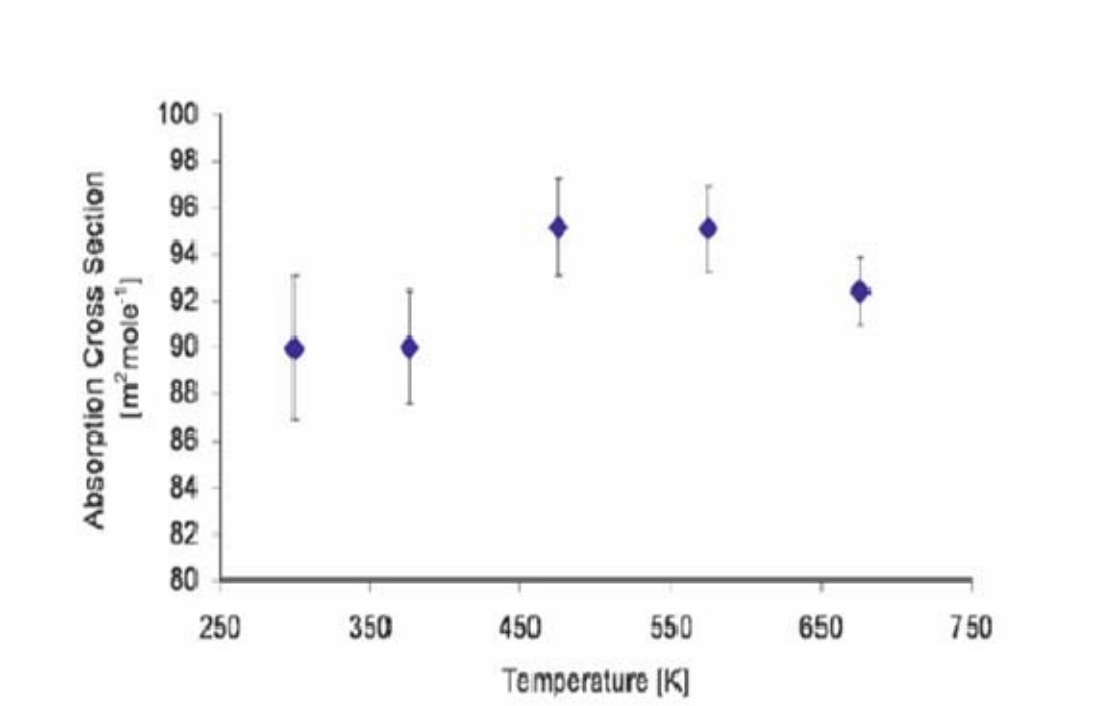

Figure 30. Absorption cross section of JP-10 at 1 atm. as a function of temperature (from [6])

C. DATA ACQUISITION AND ANALYSIS

The receiver output voltage was recorded by the control PC via a PXI-1000B expansion chassis. High speed data was acquired at 500 kHz over a two second time period and recorded voltage input to the injectors as well as voltage output from the optical receiver.

All data analysis and computation was performed using a technical computing software package called MATLAB. Individual injections were isolated and minimum and maximum voltage values for each event were determined over time and stored as data arrays. Using the minimum and maximum voltages, molar and mass fractions were calculated using Equations 26 and 27. The individual injections were then averaged to find a typical injection profile. Mass fraction curves were integrated with respect to time and multiplied by mass flow rate to determine the average mass of fuel injected per event. The MATLAB code used is included in Appendix B.

V. EXPERIMENTAL RESULTS

A. ETHYLENE

Mass fraction and equivalence ratio were determined for inlet configurations with no orifice, a single orifice plate, a multiple orifice plate and finally with a multiple orifice plate and flow conditioning screen. Each configuration was plotted vs. time. Laboratory results supported the initial CFD analysis and showed a sharper fuel delivery profile for the new multiple orifice and screen plate configuration when compared to the single orifice design. Resulting graphs for the 0.25 kg/s flow rate are shown below.

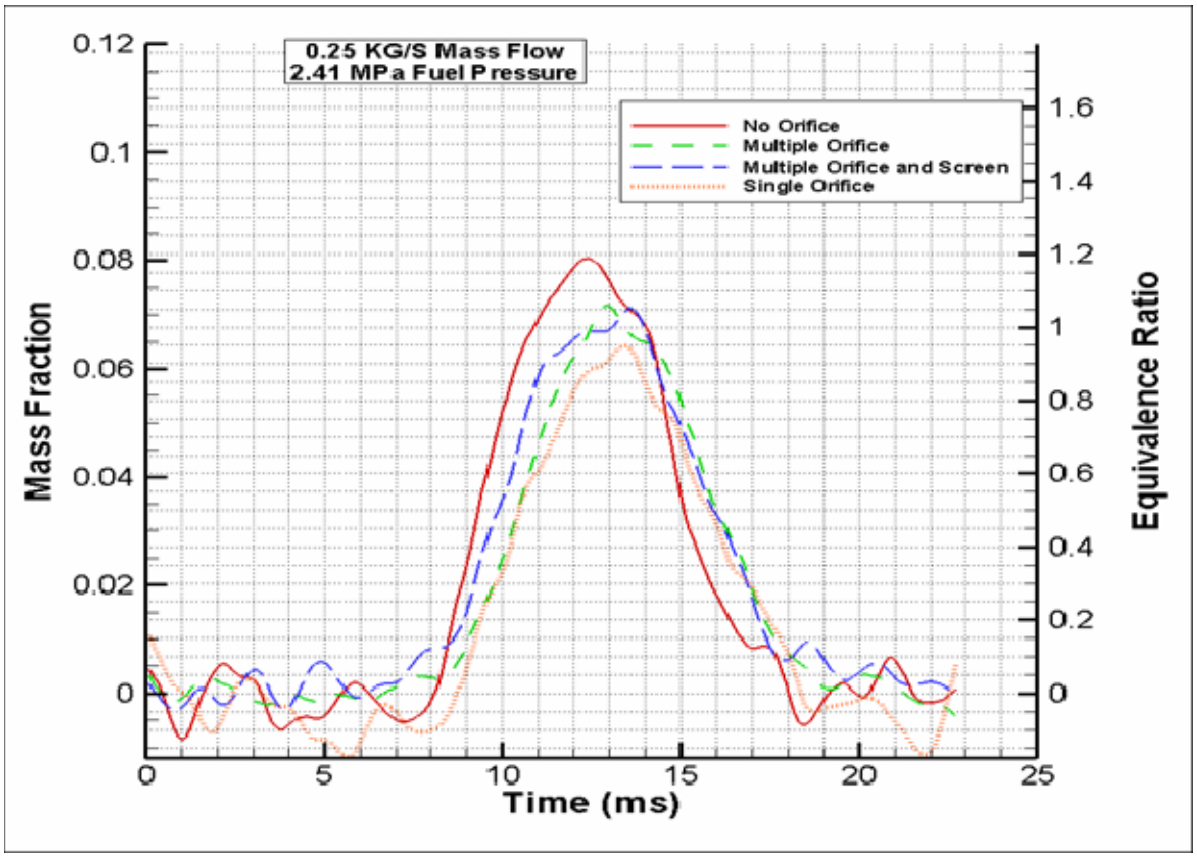

Figure 31. Ethylene mass fraction and equivalence ratio vs. time 0.25 kg/s mass flow rate, 2.41 MPA fuel pressure

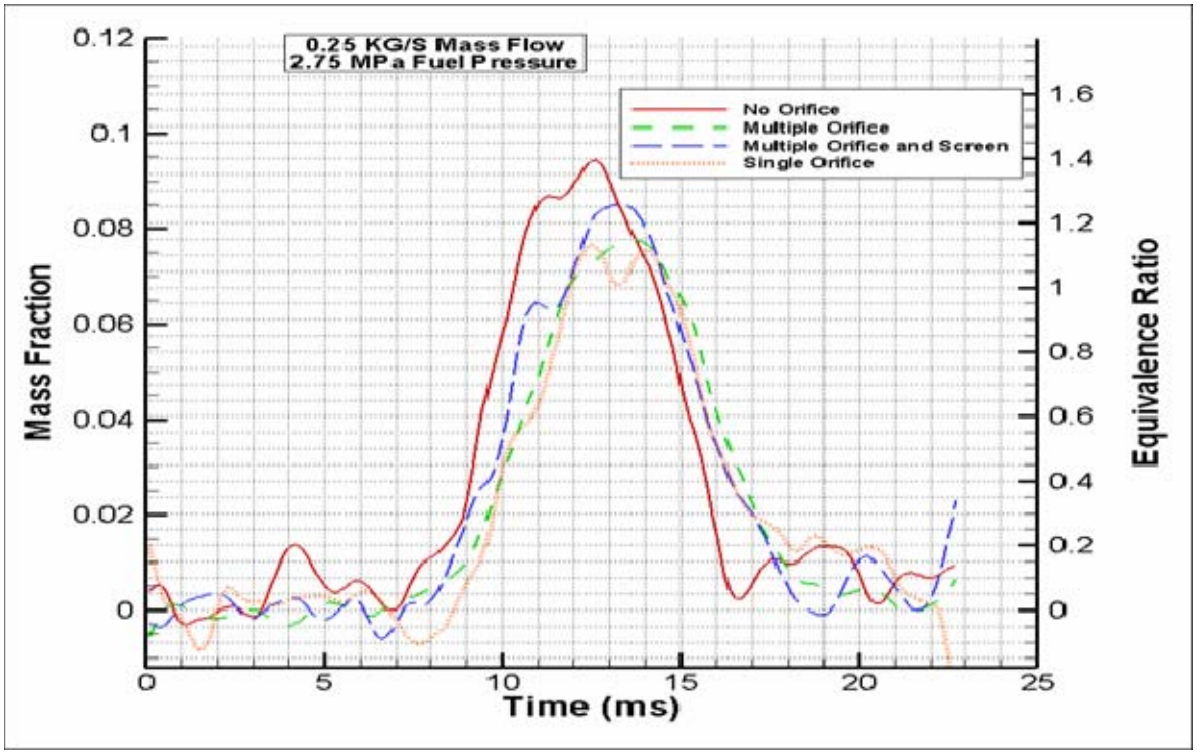

Figure 32. Ethylene mass fraction and equivalence ratio vs. time 0.25 kg/s mass flow rate, 2.75 MPA fuel pressure

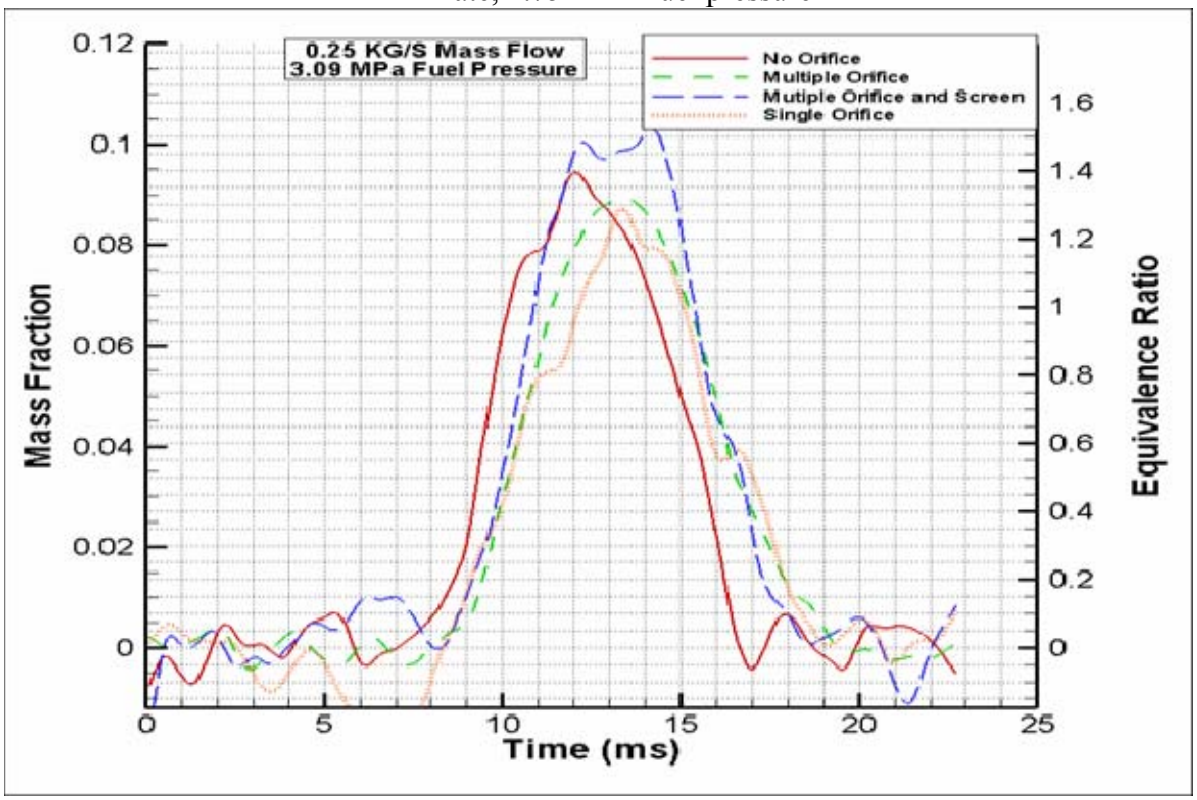

Figure 33. Ethylene mass fraction and equivalence ratio vs. time 0.25 kg/s mass flow rate, 3.09 MPA fuel pressure

Further analysis was performed on the fuel profiles to determine the amount of time for the equivalence ratio to increase from a value of 0.2 to a detonable value of approximately 0.85 after the fuel is injected, and to subsequently decrease from 0.85 to 0.2 as the fuel plug exits the combustor. Results are shown in table 7 below. Ideally, a square wave injection profile would be preferred to allow for maximum operating frequency and perfect stoichiometry for each detonation. However, due to the shape of the fluid velocity profile in the initiator tube, and the existence of recirculation zones within the engine, a square wave injection profile is not a realistic expectation. Any improvement in fuel delivery and cut-off time would tend to indicate either a flatter fluid velocity profile, a reduction in internal fluid recirculation zones in the engine, or a combination of the two.

Table 7. Ethylene fuel delivery and cutoff times at 0.25 kg/s mass flow

Air Mass Flow (kg/s)	Fuel pressure (Mpa)		Fuel Delivery (ms)		Fuel Cutoff (ms)	
			Multiple Orifice with screen	Single Orifice	Multiple Orifice with screen	Single Orifice
0.25	2.41		1.93	3.18	2.65	3.41
0.25	2.75		1.48	1.82	2.15	2.72
0.25	3.09		1.48	1.94	1.53	2.33
		AVE	**1.63**	**2.31**	**2.11**	**2.82**

The time that each configuration remained above the aforementioned detonable equivalence ratio of 0.85 was measured and is displayed in the table 8. Improvements in this duration allow for a greater percentage of the fuel injected to be consumed during each detonation event, increasing the work output and fuel efficiency of the cycle.

Table 8. Detonable fuel plug duration at 0.25 kg/s mass flow

Air Mass Flow (kg/s)	Fuel pressure (Mpa)	Time Equivalence ratio is greater than .85 (ms)			
		No Orifice	Multiple Orifice with screen	Multiple Orifice	Single Orifice
0.25	2.41	4.2	3.5	3.2	1.8
0.25	2.75	4.7	4.6	4.3	3.7
0.25	3.09	4.8	5	4.7	3.5

In each case, for the 0.25 kg/s mass flow rate, the new orifice plate geometry was superior to the single orifice design. This is consistent with the results obtained from CFD. Results for the 0.31kg/s flow rate follow.

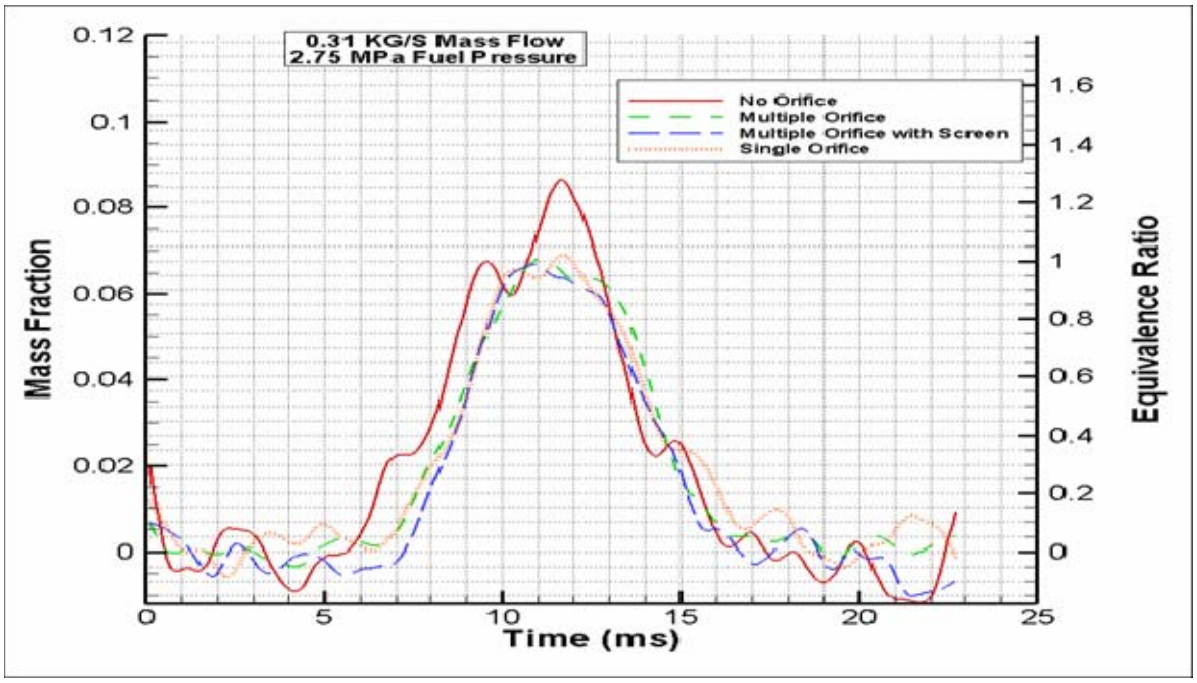

Figure 34. Ethylene mass fraction and equivalence ratio vs. time 0.31 kg/s mass flow rate, 2.75 MPA fuel pressure

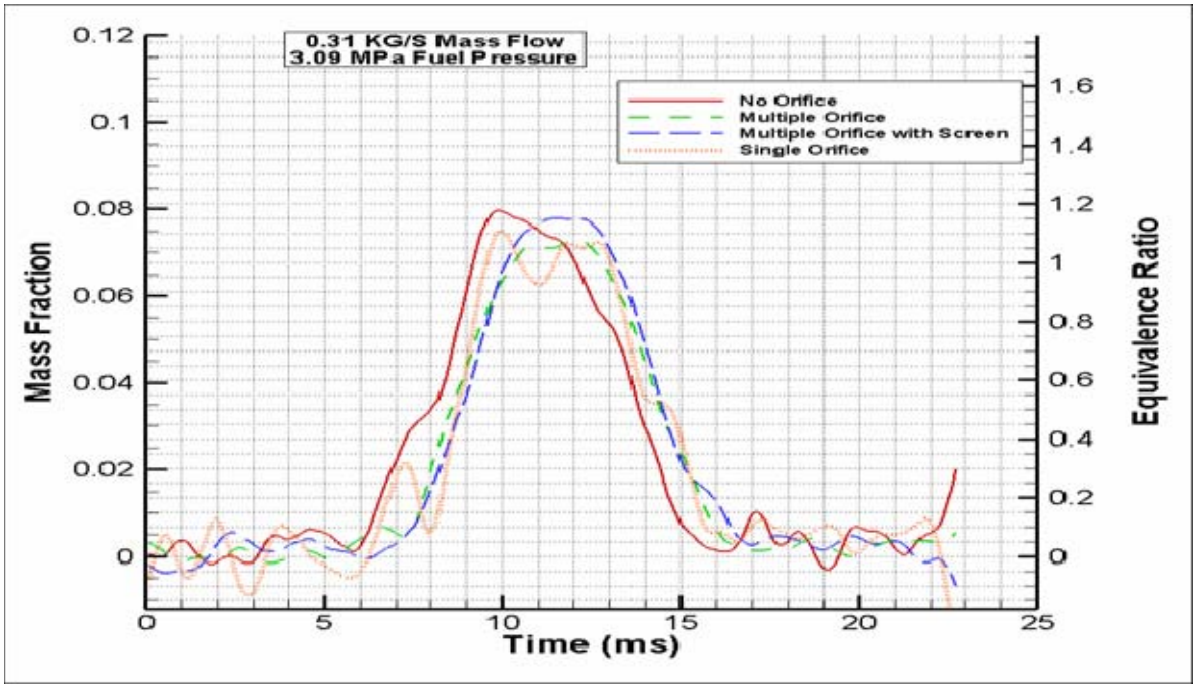

Figure 35. Ethylene mass fraction and equivalence ratio vs. time 0.31 kg/s mass flow rate, 3.09 MPA fuel pressure

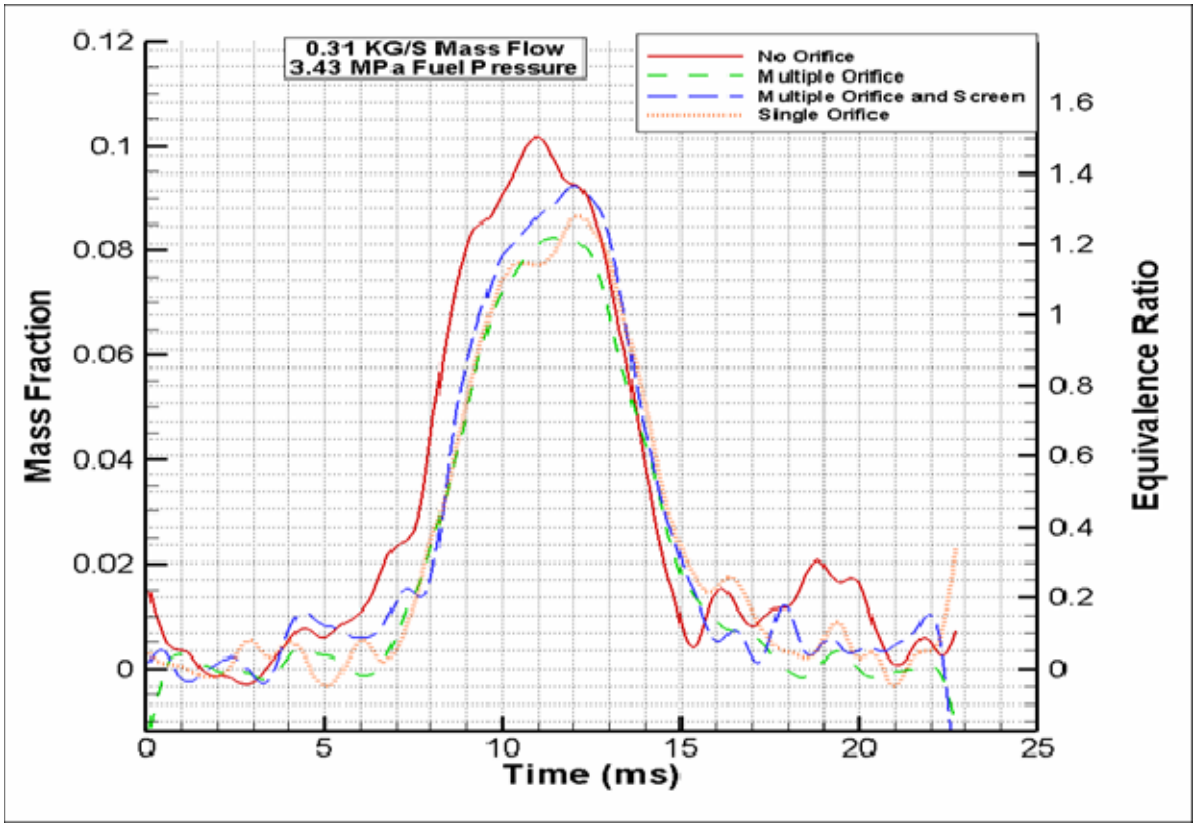

Figure 36. Ethylene mass fraction and equivalence ratio vs. time 0.31 kg/s mass flow rate, 3.43 MPA fuel pressure

Fuel delivery and cutoff times were evaluated at the 0.31 kg/s flow rate and were consistent with expected results, again showing significant improvement with the new orifice geometry.

Table 9. Ethylene fuel delivery and cutoff times at 0.31 kg/s mass flow

Air Mass Flow (kg/s)	Fuel pressure (Mpa)		Fuel Delivery (ms)		Fuel Cutoff (ms)	
			Multiple Orifice with screen	Single Orifice	Multiple Orifice with screen	Single Orifice
0.31	2.75		1.8	2	2.2	3.2
0.31	3.09		1.8	2.4	2.2	2.1
0.31	3.43		1	1.75	1.5	1.8
		AVE	**1.53**	**2.05**	**1.97**	**2.37**

Table 10. Detonable fuel plug duration at 0.31 kg/s mass flow

Air Mass Flow (kg/s)	Fuel pressure (Mpa)	Time Equivalence ratio is greater than .85 (ms)			
		No Orifice	Multiple Orifice with screen	Multiple Orifice	Single Orifice
0.31	2.75	4	3.2	3.3	3.2
0.31	3.09	3.7	4.2	3.8	4.3
0.31	3.43	5.3	4.6	4	4.3

Results for fuel plug duration were less consistent at 0.31kg/s, showing marginal improvement for the new orifice geometry. Results for the 0.35kg/s flow rate are as follows.

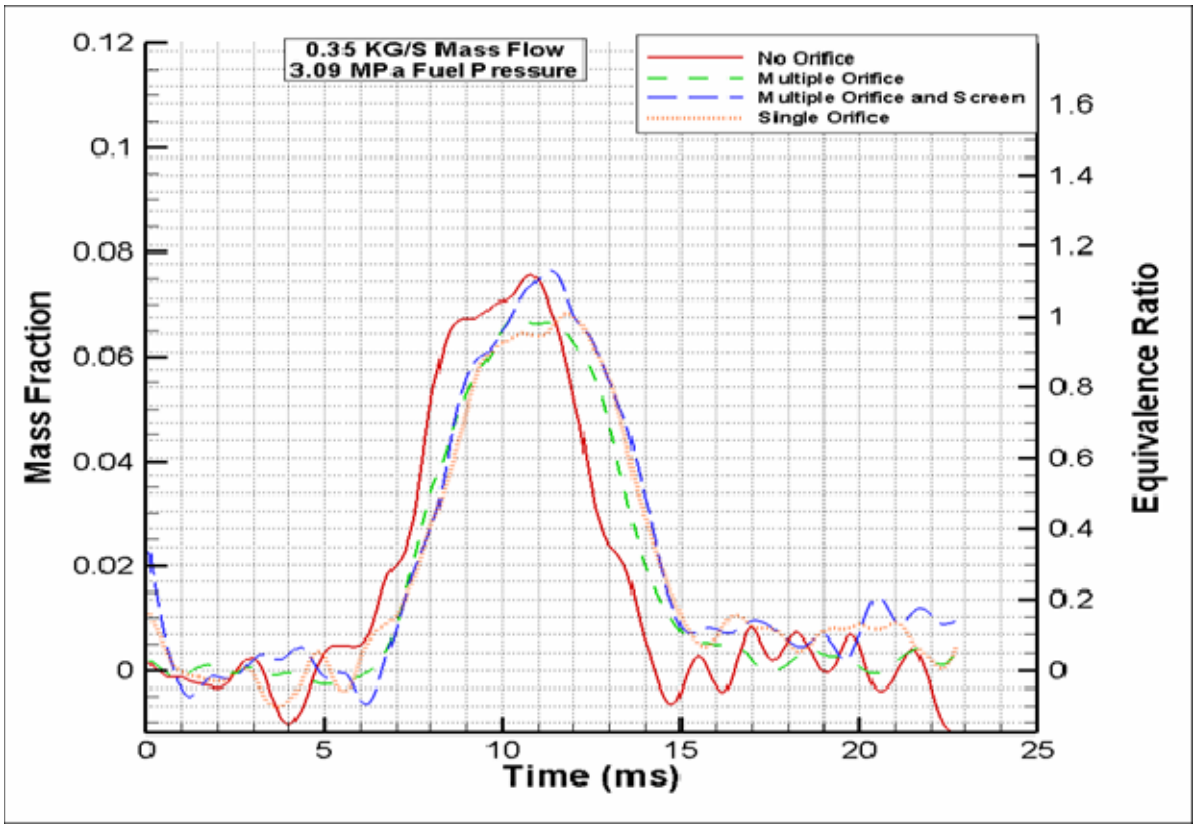

Figure 37. Ethylene mass fraction and equivalence ratio vs. time 0.35 kg/s mass flow rate, 3.09 MPA fuel pressure

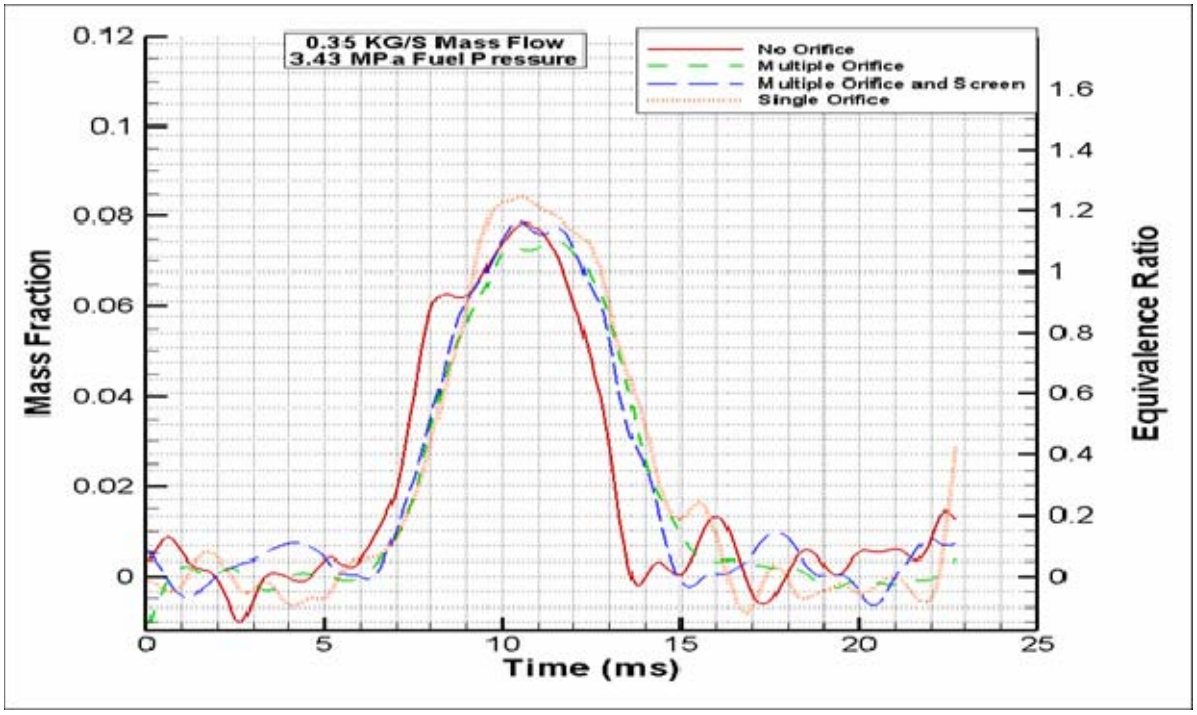

Figure 38. Ethylene mass fraction and equivalence ratio vs. time 0.35 kg/s mass flow rate, 3.43 MPA fuel pressure

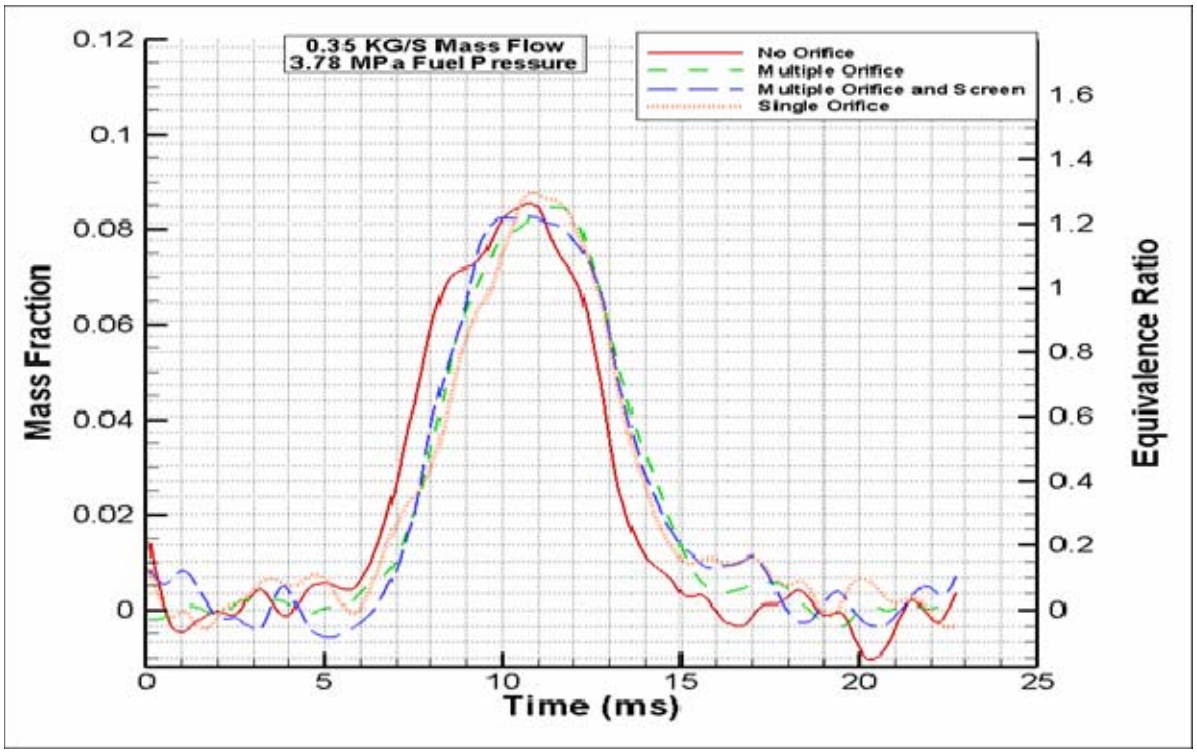

Figure 39. Ethylene mass fraction and equivalence ratio vs. time 0.35 kg/s mass flow rate, 3.78 MPA fuel pressure

Table 11. Ethylene fuel delivery and cutoff times at 0.35 kg/s mass flow

Air Mass Flow (kg/s)	Fuel pressure (Mpa)		Fuel On (ms)			Fuel off (ms)	
			Multiple Orifice with screen	Single Orifice		Multiple Orifice with screen	Single Orifice
0.35	3.09		1.7	2		1.6	1.7
0.35	3.43		1.5	1.5		1.4	1.7
0.35	3.78		1.3	2.2		2	1.8
		AVE	**1.5**	**1.9**		**1.66**	**1.73**

Fuel delivery times at the higher 0.35 kg/s mass flow rate again showed significant improvement with the new orifice design, with cutoff times showing marginal improvement. Fuel plug duration showed improvement at two of the three measured fuel pressures when compared to the original single orifice design.

Table 12. Detonable fuel plug duration at 0.35 kg/s mass flow

Air Mass Flow (kg/s)	Fuel pressure (Mpa)	Time Equivalence ratio is greater than .85 (ms)			
		No Orifice	Multiple Orifice with screen	Multiple Orifice	Single Orifice
0.35	3.09	3.7	3.8	3.1	3.6
0.35	3.43	4.3	4	3.9	4
0.35	3.78	4.5	4.3	4.3	4

Average ethylene mass injected per event was determined for each fuel pressure, flow rate and orifice configuration using a trapezoidal integration tool in MATLAB called TRAPZ. The mass fraction curves were integrated over time and then multiplied by flow rate to determine the mass of fuel injected per event. Results are shown in table 13 below.

Table 13. Ethylene mass delivered vs. fuel pressure for various engine geometries

Air Mass Flow (kg/s)	Fuel pressure (Mpa)	Ethylene mass(g)			
		No orifice	Multiple Orifice and screen	Multiple orifice	Single orifice
0.25	2.41	0.4181	0.4441	0.3974	0.2947
	2.75	0.572	0.4951	0.4629	0.4586
	3.09	0.5045	0.5988	0.5048	0.4309
0.31	2.75	0.4132	0.4201	0.3925	0.3259
	3.09	0.4741	0.4515	0.4348	0.4535
0.35	3.43	0.6507	0.555	0.4633	0.5128
	3.09	0.3653	0.4511	0.3756	0.4174
	3.43	0.4246	0.4341	0.4098	0.4335
	3.78	0.441	0.4719	0.4726	0.487

Fuel mass fraction and total fuel mass per event were also measured for six different fuel injection pressures at the .31 kg/s flow rate and was plotted vs. time and pressure respectively in Figures 40 and 41 below. Ethylene mass per injection showed a near linear increase with injection pressure which was in line with expected results.

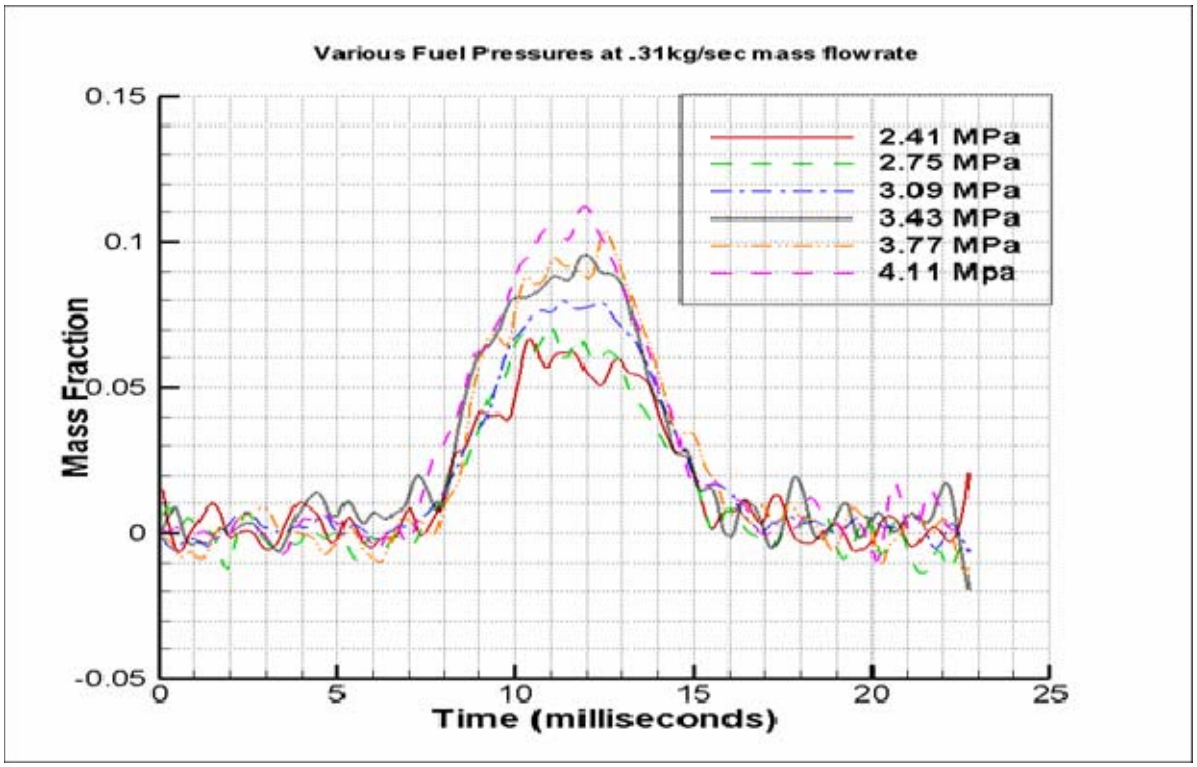

Figure 40. Various Ethylene fuel pressures at 0.31 kg/s flow rate

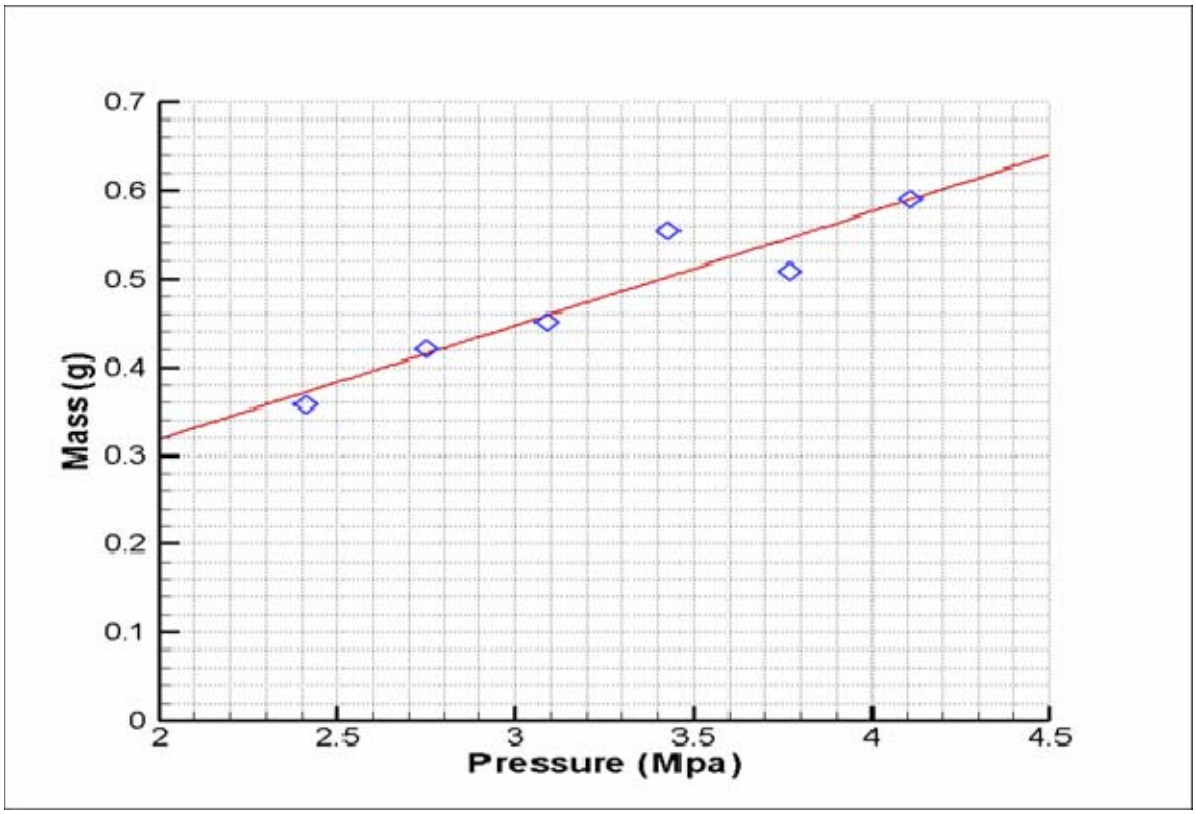

Figure 41. Ethylene mass per injection event at various pressures

B. JP10

Individual JP10 injectors were operated at 10Hz using 550 psig actuating oil pressure and their fuel profiles were plotted for comparison. Additionally two injectors were fired simultaneously at 1230 psig actuating oil pressure, and then were fired 5 ms out of phase to observe the effect on spatial fuel distribution. An individual injector profile was also plotted with a two injector profile for the purpose of comparison.

It is worth noting that the new orifice geometry was designed specifically for an injector location downstream of the orifice plate. Fluid conditions upstream of the plate where the JP10 injectors are located were not evaluated using CFD and the laboratory results suggest there may be significant fuel recirculation upstream of the plate, and/or liquid fuel impingement on the piping wall, indicated by the length of time required for

the fuel mass fraction to decrease from its peak value back to a value near zero. Fuel delivery was crisp however, typically approaching a peak value two to three ms after it reached the exit plane of the PDE.

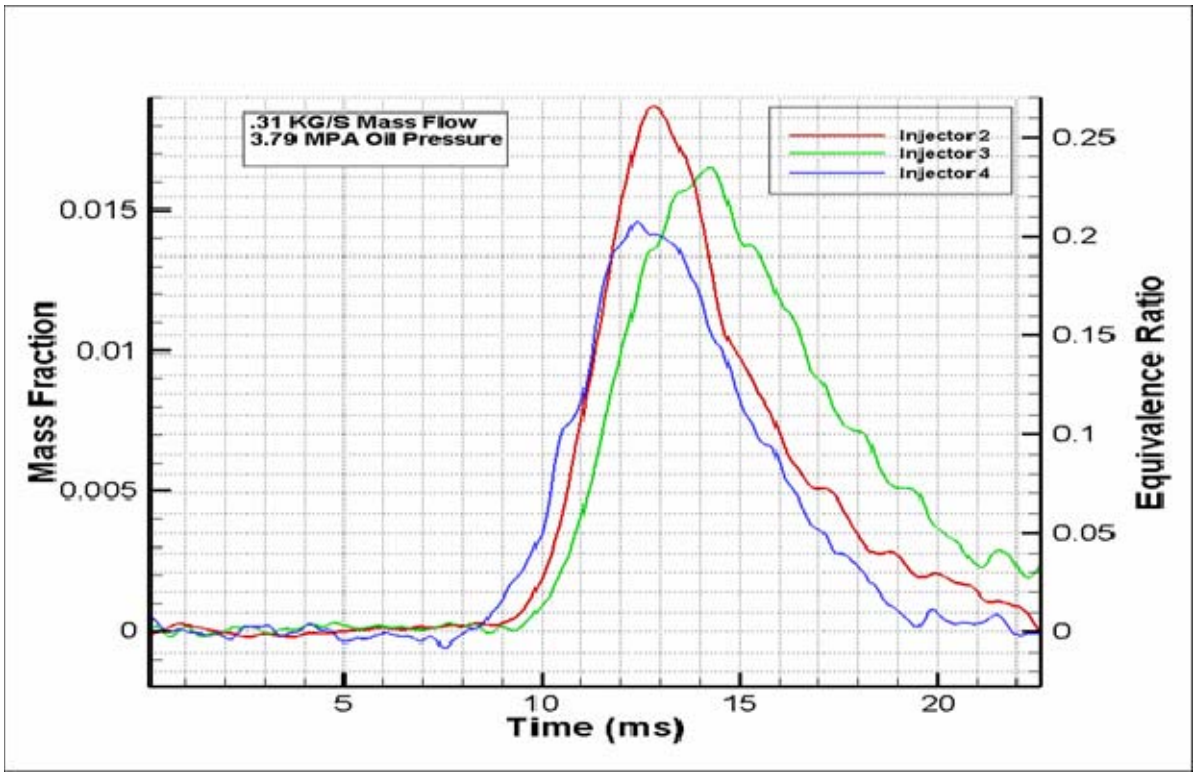

Figure 42. JP10 individual injector fuel profiles at 550 psig actuating oil pressure

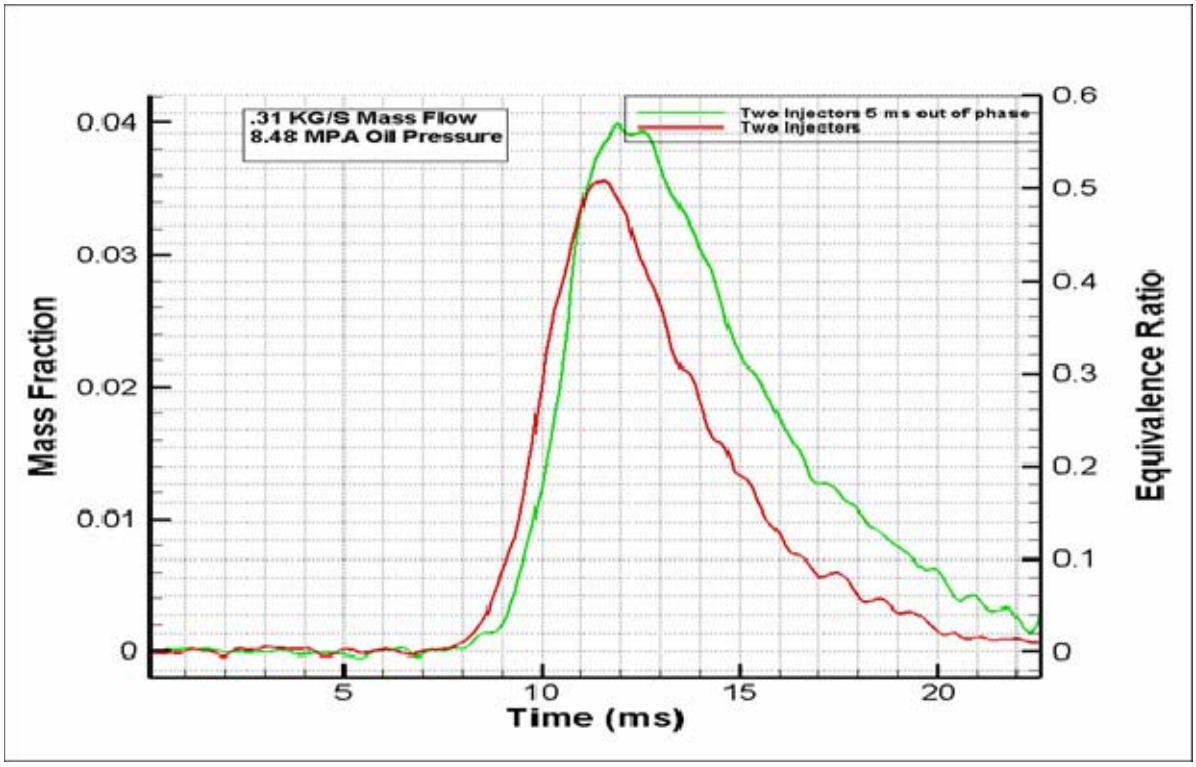

Figure 43. JP10 fuel profiles for in phase and 5 ms out of phase injections using two injectors at 1230 psig actuating oil pressure

Results for the single injectors were relatively consistent, with slight variations in fuel delivery time and equivalence ratios for each. Results for the multiple injector plots were as expected in terms of fuel timing, showing increased fuel plug duration for the out of phase injectors. In terms of mass fraction however the results were unexpected, with the out of phase injectors showing an increased mass fraction and fuel mass delivered to the exit plane of the PDE when compared to the in phase injectors.

A comparison of a single injector at 550 psig actuating oil pressure vs. two injectors with a 1230 psig actuating oil pressure is shown in Figure 45 and is consistent with expected results. Injector piston actuation time is reduced at the higher 1230 psig oil pressure, resulting in a faster, sharper fuel delivery profile. Additionally the mass fraction and equivalence ratio for the multiple injector events is on the order of two times that of the single injector.

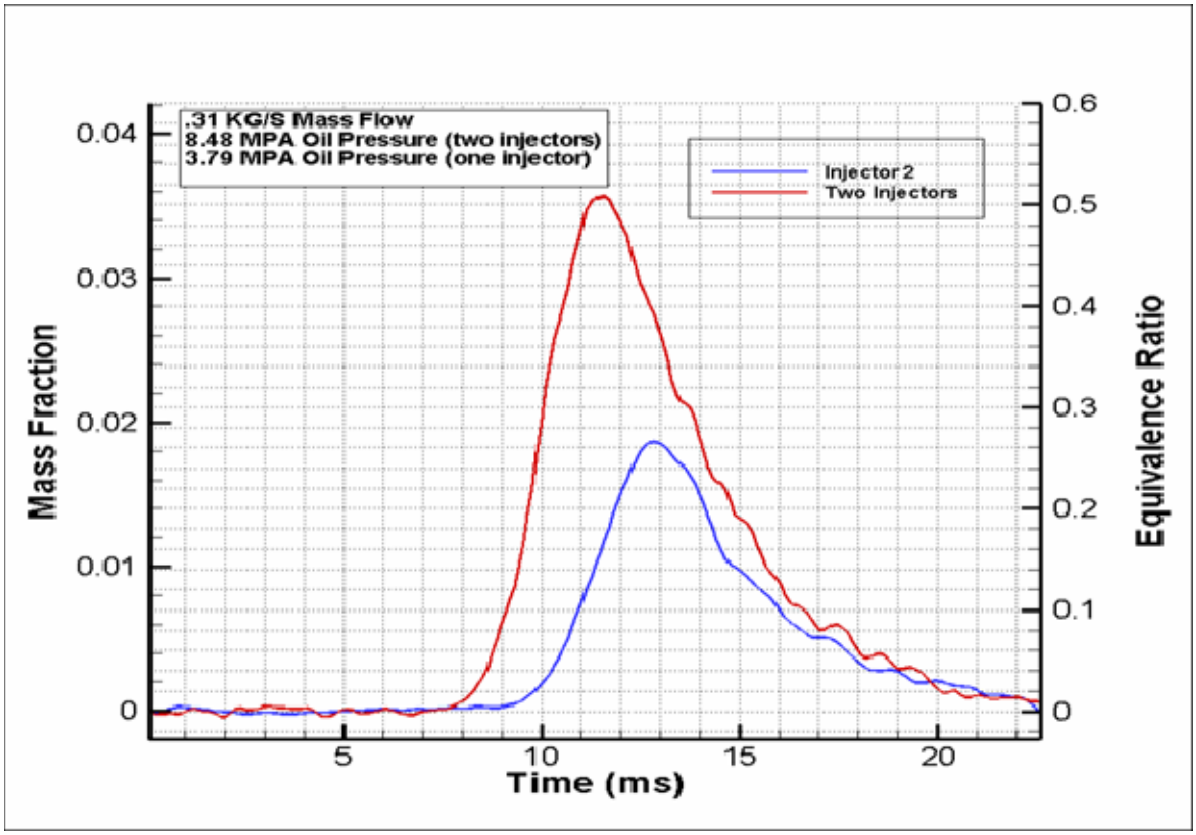

Figure 44. JP10 fuel profile comparison for a single injector using 550 psig actuating oil pressure vs. two injectors using 1230 psig actuating pressure

Fuel mass was determined for JP10 using the same methodology implemented for ethylene. Results are tabulated below in Table 14. Injector specifications state that each injector will inject 130 ml^3 of fuel which corresponds to 0.122 grams of fuel per injection event. Previous research at NPS has suggested that liquid fuel impingement on piping walls may inhibit the effective atomization of the liquid fuel into the air stream which would have the effect of reducing the mass measured at the outlet of the PDE [13]. Taking this into consideration, combined with the suspected existence of an area of turbulence upstream of the orifice plate, the results for individual injectors seem reasonable. The out of phase two injector results track closely with injector specifications, while the in phase measurement, as noted earlier in this paper, is slightly lower.

Table 14. JP10 fuel mass for various injector configurations

Oil Pressure(Mpa)	Injectors	JP10 Mass(g)
3.79	Injector 2	0.0902
	Injector 3	0.1028
	Injector 4	0.0744
8.48	Injectors 2 and 4	0.1778
	Injectors 1 and 3 five ms out of phase	0.2381
	Injectors 2 and 4 five ms out of phase	0.2511

VI. CONCLUSIONS

A. SUMMARY

Work performed during this thesis demonstrated the ability to effectively measure ethylene and JP10 fuel mass fractions and fuel mass during simulated in-flight conditions using a 3.39 μm Helium-Neon laser. Implementing known fuel absorption cross sections and absorption spectroscopy techniques discussed earlier in this thesis, spatial fuel distributions along the PDE axis were evaluated and presented in the form of time-resolved fuel mass fraction graphs. These fuel distribution graphs eliminate the necessity of trying to predict spatial fuel distribution and mass fraction during operation and improve the ability to achieve reliable detonations. Accurate aggregate fuel mass measurements directly enhance the ability to accurately calculate engine performance characteristics.

Additionally, fluid conditions across the inlet orifice of the engine were modeled in an effort to determine flow conditions downstream of the plate after pre-ignition of injected fuel was observed during operation. This modeling lead to the design of a new inlet plate geometry in a simultaneous effort to eliminate the observed pre-ignition while improving fuel injection profiles for the PDE. The resulting design demonstrated improved fuel delivery profiles during both computer modeling and during laboratory evaluation with the ethylene fuel.

B. RECOMMENDATIONS

While the ability to measure the spatial distribution and mass fraction of the JP10 fuel has been demonstrated, the fuel distribution profile produced by the existing engine inlet geometry is not ideal. The location of the fuel injectors directly upstream of the inlet orifice plate likely degrades fuel delivery due to existing recirculation zones in the area and due to increased liquid fuel impingement on piping walls and the orifice plate itself. The planned relocation of the injectors downstream of the orifice plate should resolve this issue.

Future efforts in this area should focus on the ability to measure fuel mass and spatial distribution in real time during engine operation. This ability, integrated with an automated controls system to adjust fuel pressure and injection duration during operation, will dramatically improve the ability to achieve reliable detonations.

APPENDIX A. ORIFICE PLATE DESIGN SPECIFICATIONS

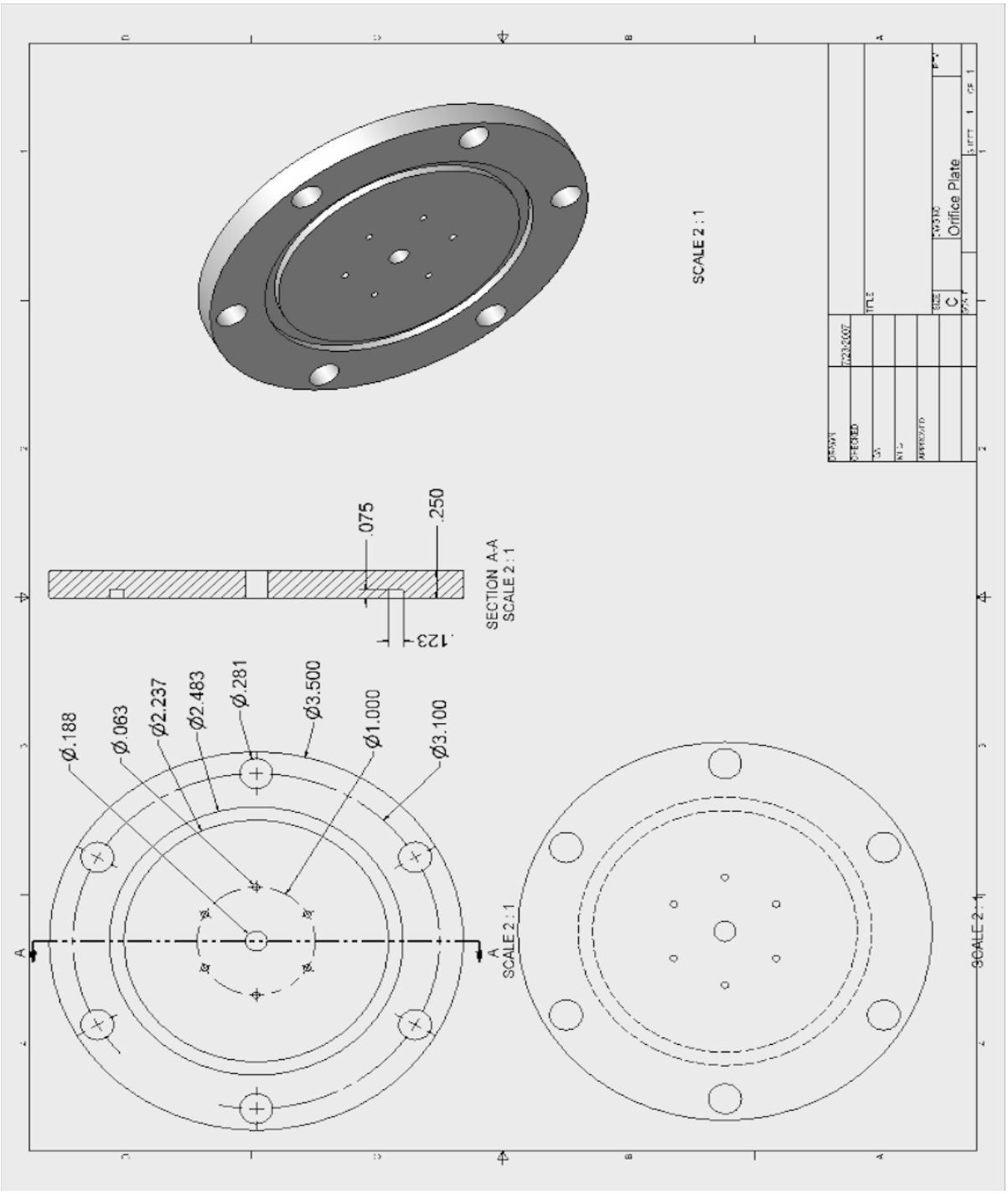

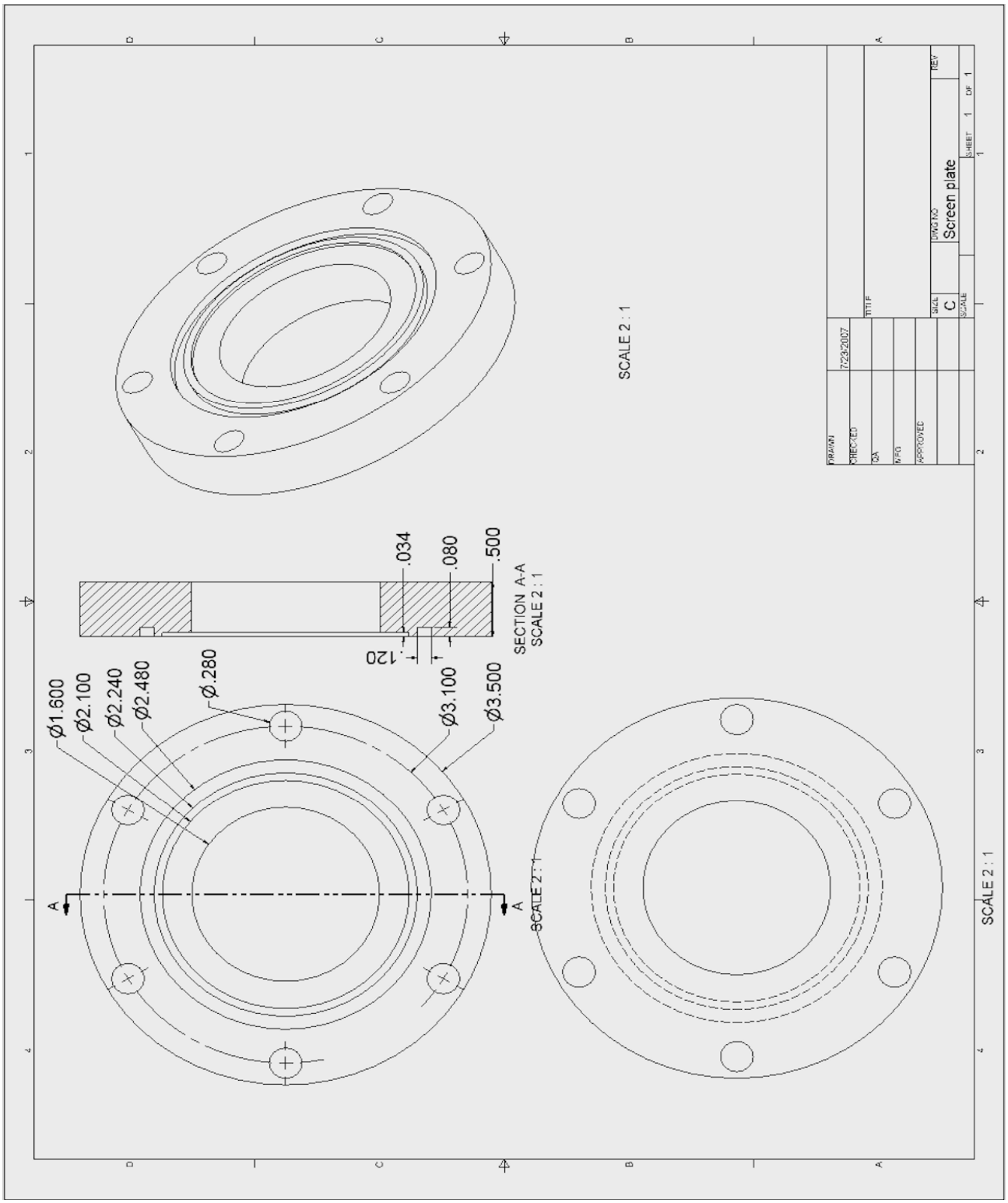
Ø1.600
Ø2.100
Ø2.240
Ø2.480
Ø.280
Ø3.100
Ø3.500
.034
.080
.500
.120
SECTION A-A
SCALE 2 : 1
SCALE 2 : 1
SCALE 2 : 1
SCALE 2 : 1
DRAWN
CHECKED
QA
MFG
APPROVED
7/23/2007
TITLE
SIZE
C
DWG NO
Screen plate
REV
SCALE
SHEET 1 OF 1

APPENDIX B. MATLAB CODE

```
%The purpose of this program is to convert the raw data from the IR
%receiver output to fuel mass fraction profiles using a form of the
%Beer-Lambert Law.

clc
clear

%Load Data and define variables

z=mydata(:,1);
x=(mydata(:,2)-.2);
[n,p]=size(mydata)
t=1:n;

%Find fuel valve open signal
fuelon=find(z>=3);

%determine interval between events
[a,b]=find (diff(fuelon)>2);
size([a,b]);
I=50000;

%determine frequency
f=(n/2)/(I);

%find number of injection events
Ni=length(a);

%find time of first injection event
A=fuelon(1,1);

%Set sampling time
St=28000;

%Define Arrays representing each injection event
  for N=1:(Ni)
     C(:,N)=([x((A+(N-1)*I):(A+(N-1)*I+St))]);

  end

%Find local minimums for each array

for v=1:Ni;
c1=C(:,v);
thresh = 0;
N = length(c1);

%Find zero crossings

zc = (sign(c1) >= thresh) - (sign(c1) < thresh);
b=find((zc(1:N-1) - zc(2:N)) ~= 0);
start=c1(b(1));
```

```
[nn,pp]=size(b);
over=c1(b(nn));

if sign(start)<0&&sign(over)>0;
  n1=0;
  e1=nn;
else if sign(start)<0&&sign(over)<0;
    n1=0;
    e1=(nn-1);
    else if sign(start)>0&&sign(over)<0;
           n1=1;
           e1=(nn-1);
        else if sign(start)>0&&sign(over)>0;
               n1=1;
               e1=nn;
            end
        end
    end
end
arrays=(e1-n1)/2
if arrays>200;
    arrays=200;
end
for NN=(1:((arrays)-1));
    %capture negative arrays
   CC((b(2*NN-n1)):(b(2*NN-n1+1)),NN)=([c1((b(2*NN-n1)):(b(2*NN-
n1+1)))]);
   %capture positive arrays
   MM((b(2*NN-n1+1)):(b(2*NN-n1+2)),NN)=([c1((b(2*NN-n1+1)):(b(2*NN-
n1+2)))]);
end

%Find maximums
Max=[max(MM)];
j(:,v)=[Max];
Max_ave=sum(mean(j)/(Ni));

%Find minimums
l=[min(CC)];
s(:,v)=([l]);

end
for h=1:199;
kp(:,h)=sum(s(h,:));
end

%Determine minimums and average minimums for series of injection events
Mins=kp;
Min_ave=(Mins/(Ni));

%Determine baseline value for minimums
M=mean(Min_ave((1):(30)));

%Determine a baseline voltage difference(Io)
Delta_Vb=abs(M-Max_ave);
```

```
%Now determine voltage difference for the entire injection event(I)
Delta_Vi=abs(Min_ave-Max_ave);

%Divide to get voltage ratio
Ratio_V=Delta_Vi/Delta_Vb;


%Determine Molar Fraction
%Xi=molar fraction
%Ratio_V=I/Io
%Universal Gas constant =8.314472
%Degrees Kelvin
%Absorption Cross Section=.7 ethylene, = 92 JP10
%Pressure = Patm = 101325 Pa
%Length=Diameter of outlet = .089 Meters

Xi=[(-(log(Ratio_V))*8.314472*422*100)/(92*101325*8.89)];

%Determine total mass of fuel

%Xm=mass fraction

%Xm=(Xi./(1-Xi))*(28.05/28.8);%Ethylene
Xm=(Xi./(1-Xi))*(136.237/28.8);%JP10
```

THIS PAGE INTENTIONALLY LEFT BLANK

APPENDIX C. TEST CELL TWO STANDARD OPERATING PROCEDURE

Test Cell #2
Standard Operating Procedures (S.O.P)
Engine Start UP

Prior to starting preparations

1. Notify all lab personnel of live test cell.
2. Turn ON control console
3. Turn ON warning lights
4. Notify the Golf Course (x2167, ext#1) (Only required if Hot Fire Test is conducted)

Preparing Test Cell

1. Push the Emergency Stop IN (secured)
2. Turn ON BNC Cabinet Power Strip.
3. On Control Computer, open LABVIEW and ensure that the execution target contains the PXI address. Open control panel and run the program.
    a. RT Target address: 172.20.120.118
    b. Control Program Path
        i. Open
        ii. Test Cell #2 Manual Control v20 (runs v19b)
        iii. Enter Run Path Name
            1. If this is not completed prior to running you will lose the data file that was created with the default name.
4. Turn ON 24 VDC in the control room cabinet
5. OPEN Main Air (HP Air Tank Valve) and High Pressure Air
    a. Blue hand valve should be opened slowly as not to shock the lines
    b. Node 4 air valve in test cell #1 open
6. OPEN H_2 & O_2 six packs
7. Enter Test Cell #2 and OPEN all the supply gas bottles that are going to be used
8. OPEN both JP-10 valves
9. Ensure that PXI Controllers, Kistlers, and Power strip in the black cabinet are ON.
10. Turn ON 24 VDC power supply for Test Cell #2 TESCOM Control Power.
11. OPEN Shop Air, Isolation Valve(High Pressure Air) and Main Air
12. If JP-10
    a. CLOSE 440 VAC knife switch for Oil Pump
13. TURN ON Cooling Water
14. TURN ON TPI (do not exceed 85 on heater control knob) – 30-60-80 (1 min intervals)
15. CONNECT Vitiator Spark Plug (if being used).
16. If required, set up any visual data recording equipment.
17. Evacuate all non-essential personnel to the control room

18. Check Shop Air Compressor in heater room– approx 120 psi min
19. RUN the control
20. Close Blast Door
21. Lock Gate

Running the Engine

1. Set Main Air, Secondary/Purge Air, and all other gas pressures (ER3000) ON RPL00
    a. Set Main Air and Purge Air (ER3000)
        i. 001 Main Air
        ii. 004 Secondary Air – Set to 220
    b. Supply Gases in Test Cell #2 TESCOM Node Address
        i. 020 Vit H_20
        ii. 21 Vit O_2
        iii. 22 C_2H_4
2. **DISCONNECT CH 7 & 8**
3. Set All Engine Control Parameters (on BNC Pulse Generator)
    a. Send Engine Parameters to BNC
4. **RECONNECT CH 7 & 8**
5. Twist Emergency Stop Button clockwise (TEST CELL IS NOW LIVE)
6. ENABLE the Test Cell on the VI.
7. OPEN Vit, Torch, and C_2H_4 Ball Valves.
8. Verify Golf Course is clear
9. Sound the Siren
10. When area is clear, START record VCRs
11. Fuel Pump On
12. TURN ON Data Recording Switch
13. Manually engage Main Air flow
14. Start Vitiator

**********WARNING**********

The next step will result in the commencement of a run profile and ignition.

* Note: The 3-Way Ball Valve has a control in the Vitiator sequence. If the Vitiator is used then the 3-Way Ball will not divert through the engine until 375º F and will dump overboard at the end of the run at 175º F.

15. COMMENCE RUN
    a. High Speed DAQ will be triggered and the engine profile will commence
16. STOP RUN.
    a. Pulse generation will be stopped.
17. TURN OFF Data Recording Switch
18. Wait for main air to divert
19. Stop Main Air Flow
20. Ensure all BV are closed
21. Fuel pump off
22. DISABLE the Test Cell on the VI.
23. Push Emergency Stop Button IN

Test Cell #2
Standard Operating Procedures (S.O.P)
Engine Shut DOWN

1. SET all supply gases to ZERO, Nodes 1,4,20, 21 &22
2. CLOSE all gas supply valves using Labview
3. STOP control code.
4. Push Emergency Stop Button IN
5. Turn OFF Power Strip in BNC Timing Cabinet
6. If Gas Turbine Igniter used DISABLE BEFORE turning off 24 VDC
7. TURN OFF 24 VDC power supply (check with other test cells first)
8. CLOSE Jamesbury Valve (check with other test cells first)
9. REMOVE Vitiator Spark Plug head
10. SECURE TESCOM 24VDC power. (check with other test cells first)
11. CLOSE Shop Air, High Pressure Air, and Main Air
12. If using JP-10
    a. CLOSE 440 VAC Knife switch
13. TURN OFF Cooling Water
14. CLOSE Supply gases
15. CLOSE JP-10 supply valves
16. TURN OFF TPI
17. CLOSE H_2 & O_2 six packs
18. VENT H_2 & O_2 lines
19. STOW Cameras and other equipment used in testing.
20. CLOSE Test Cell #2.
21. TURN OFF Warning Lights.

THIS PAGE INTENTIONALLY LEFT BLANK

LIST OF REFERENCES

[1] S. Eidelman, and W. Grossman. "Pulsed Detonation Engine Experimental and Theoretical Review," AIAA/SAE/ASME/ASEE 28th Joint Propulsion Conference and Exhibit, Nashville TN, 6-8 July 1992. Paper no. AIAA 92-3169.

[2] R. Friedman, "American Rocket Society," Vol. 24, p.349, November 1953.

[3] Cequel™ Chemical Equilibrium in Excel. Version 1.75, Carson City, Nevada, Software and Engineering Associates, Inc.

[4] K. Kuo. *Principles of Combustion,* Second Edition, John Wiley and Sons, 2005.

[5] I. Glassman. *Combustion*, Second Edition, Academic Press, Inc., 1987.

[6] A. E. Klingbeil, J. B. Jeffries, and R. K. Hanson. "Temperature- and Pressure-Dependant Absorption Cross Sections of Gaseous Hydrocarbons at 3.39 μ m" Measurement Science and Technology, Vol. 17, 12 June 2006.

[7] H. Hoffmann. "Reaction-Propulsion Produced by Intermittent Detonative Combustion," German Research Institute for Gliding, Report ATI-52365, August 1940.

[8] F. Ma, J. Choi, and V. Yang. "Propulsive Performance of Airbreathing Pulse Detonation Engines," Journal of Propulsion and Power, Vol. 22, No. 6, November-December 2006.

[9] C. M. Brophy, and R. K. Hanson. "Fuel Distribution Effects on Pulse Detonation Engine Operation and Performance," Journal of Propulsion and Power, Vol. 22, No. 6, November-December 2006.

[10] Y. Wu, F. Ma, and V. Yang. "System Performance and Thermodynamic Cycle Analysis of Airbreathing Pulse Detonation Engines," Journal of Propulsion and Power, Vol. 19, No. 4, July-August 2003.

[11] C. Brophy, S. Werner, and J. Sinibaldi. "Performance Characterization of a Valveless Pulse Detonation Engine," AIAA paper 2003-1344, *41st Aerospace Sciences Meeting and Exhibit*, Reno, Nevada, 6-9 January 2003.

[12] E. Wintenberger, and J. E. Shepherd. "Thermodynamic Analysis of Combustion Processes For Propulsion Systems," AIAA paper 2004-1033, *42nd Aerospace Sciences Meeting and Exhibit*, Reno, Nevada, 5-8 January 2004.

[13] P. E. Damphousse. “Characterization and Performance of a Liquid-Hydrocarbon Fueled Pulse Detonation Rocket Engine,” M.S. Thesis, Naval Postgraduate School, Monterey, California, December 2001.

[14] CFD-ACE Modules Manual. Version 2004, Huntsville, Alabama: ESI CFD, Inc.

[15] CFD-FASTRAN Theory Manual. Version 2004, Huntsville, Alabama: ESI CFD, Inc.

INITIAL DISTRIBUTION LIST

1. Defense Technical Information Center
   Ft. Belvoir, Virginia

2. Dudley Knox Library
   Naval Postgraduate School
   Monterey, California

3. Professor Chris Brophy
   Naval Post Graduate School
   Monterey, California

4. Professor Jose Sinibaldi
   Naval Post Graduate School
   Monterey, California

5. LT Tom Danaher
   Gloucester, Virginia